REPORT DOCUMENTATION PAGE

Form Approved
OMB No. 0704-0188

1. AGENCY USE ONLY (Leave blank)	2. REPORT DATE	3. REPORT TYPE AND DATES COVERED
	September 1995	Final, 1 Jul 92 - 31 Jul 95

4. TITLE AND SUBTITLE
Synthesis, Characterization, and Properties of Nanometer-sized Intermetallics

5. FUNDING NUMBERS
F49620-92-J-0252

AFOSR-TR-96 97

0034

6. AUTHOR(S)
Marek Dollar, Mahmood S. Choudry

7. PERFORMING ORGANIZATION NAME(S) AND ADDRESS(ES)

Metallurgical Engineering and Materials Science
Illinois Institute of Technology
Chigaco, IL 60616

REPORT NUMBER

9. SPONSORING / MONITORING AGENCY NAME(S) AND ADDRESS(ES)
Air Force Office of Scientific Research
AFOSR/NA
110 Duncan Ave, Suite B115
Bolling AFB DC 20332-8080

10. SPONSORING / MONITORING AGENCY REPORT NUMBER

11. SUPPLEMENTARY NOTES

12a. DISTRIBUTION AVAILABILITY STATEMENT

Approved for public release, distribution is unlimited.

12b. DISTRIBUTION CODE

13. ABSTRACT *(Maximum 200 words)*

Nanocrystalline intermetallics were produced from pre-cast NiAl using electron beam inert gas condensation system. A liquid nitrogen cooled cold finger was used to collect the powder. After collection, the powder was transported under high vacuum to a compaction unit where in-situ compaction at 1.4 Gpa was carried out under vacuum conditions at temperatures ranging from 100 to 300C. Energy dispersive spectroscopy and X-ray diffraction (XRD) techniques were used to investigate chemical composition, phase and grain size. Average grain size in the range of 2 to 10 nm was found for various specimens. XRD spectra of as consolidated specimens suggested a majority of ordered phase with little disordering in n-NiAl.

19970117 059

14. SUBJECT TERMS
Nickel aluminide, nanocrystalline, nanophase

15. NUMBER OF PAGES
81

16. PRICE CODE

17. SECURITY CLASSIFICATION OF REPORT	18. SECURITY CLASSIFICATION OF THIS PAGE	19. SECURITY CLASSIFICATION OF ABSTRACT	20. LIMITATION OF ABSTRACT
UNCLASSIFIED	UNCLASSIFIED	UNCLASSIFIED	UNLIMITED

Rcvd 960603
Accepted 960612

SYNTHESIS, CHARACTERIZATION, AND PROPERTIES OF NANOMETER-SIZED INTERMETALLICS

FINAL TECHNICAL REPORT

MAY 1996

PREPARED: PROF. MAREK DOLLAR, Principal Investigator
MAHMOOD S. CHOUDRY, PhD Student

TABLE OF CONTENTS

ABSTRACT

Intermetallic compounds (Ni Aluminide) have superior properties at high temperature but lack low temperature strength and ductility. The aim of this research is to investigate low temperature properties of aluminides with grain size in the nanometer regime.

Nanocrystalline intermetallics have been produced from pre-cast NiAl using an electron beam inert gas condensation system. A liquid nitrogen cooled cold finger was used to collect the powder. After collection, the powder was transported under high vacuum to a compaction unit where in situ compaction at ~ 1.4 GPa was carried out under vacuum conditions at temperature ranging from 100 to 300 ^{o}C

Energy dispersive spectroscopy and X-Ray diffraction (XRD) techniques were used to investigate chemical composition, phase and grain size. Average grain size in the range of 2 to 10 nm was found for various specimens. XRD spectra of as consolidated specimens suggested a majority of ordered phase with little disordering in n-NiAl.

The density of the compacts were obtained by Archemedes principal and it was correlated with the non-stoichiometric composition and the die compaction temperature. Densities ranging from 70% to 90% of the theoretical were achieved in the as-compacted state.

Scanning electron microscopy (SEM) was done to perform chemical analysis by EDS. Chemical composition of most of the samples were found within the single phase region of NiAl. Also SEM and optical microscopy was done to analyze surface structure features such as defects, cracks, inhomogenity, porosity, and surface finish.

1. INTRODUCTION:

Nanocrystalline materials as from its name implied are composed of grains with dimensions in nanometer regime. First nanocrystalline material with grain size less than 100 nm was prepared by Gleiter et al.[1-3] Any material with particles in nanometer range (> 100 nm) consists of nanoscale clusters. Such nanoscale clusters do not respond to either free atoms or molecules making up the particles or bulk material with similar composition with respect to physical properties.

Since these clusters are very small therefore they have large surface to volume ratio which resulted in large number of atoms residing in grain boundaries. The variation of grain boundary area with respect to grain size in nanoscale materials can be seen in figure 1.[4] Metastable phases can therefore be generated in materials with grain dimensions in nanometer range which are different from those of the bulk.

A schematic representation of hard sphere model of a nanocrystalline material is shown in figure 2.[5] In this hard sphere model all the atoms (filled circles and open circles) are chemically identical. But two kinds of atoms can be identified based of atomic structure. One type of atom form crystal lattice (filled circles) in which nearest neighbor configuration responds to a lattice arrangement. The second type of atoms (open circles) form random

arrangement in which the nearest neighbor configuration corresponds to boundary arrangement. Therefore nanocrystalline materials can be classified as materials consisting of crystalline component surrounded by interfacial component called grain boundary area.

The field of nanophase materials have generated considerable attention during the past few years. Many investigators have developed various techniques to synthesize nanophase clusters of different systems. But currently most of the attention have been given to synthesize clusters prepared by gas phase condensation. Such technique has the advantage of providing a substrate free configuration for the nanoscale particles, which can be compacted to produce bulk materials. The average grain size in these materials produced by this technique range from 2 to 50 nm on average. The properties related to such materials, synthesized so far are different from those of the coarse grained counter parts of the same chemical composition. In some materials, some of the properties showed a marked improvement over the coarse grained counter parts. By changing the initial composition and processing variables, the atomic arrangement at the interfaces can be varied to obtain different metastable configurations thus resulting in a wide variety of materials novel properties.[6] Such properties involved enhanced diffusion, increased specific heat, decreased Debye temperature, increased coefficient of thermal expansion, solubility and alloying of previously

immiscible elements, increased ductility in compression, improved tensile strength, and increased micro hardness.[6-14]

2. NANOCRYSTALLINE NIAL POWDER SYNTHESIS AND CONSOLIDATION:

2.1. INERT GAS CONDENSATION:

2.1.1. INTRODUCTION:

Inert gas condensation is a method which can produce clusters of atoms with sizes less than 100 nm. In this method small particles with very high purity can be produced with good crystallinity and clean surfaces. Inert gas condensation is a physical method of synthesizing materials with no chemical reaction. The evaporation source associated with the Inert gas condensation system can be varied. The current up to date methods are resistive heating, electron beam evaporation, arc discharge and laser ablation. In addition to Inert gas condensation method there are other methods such as high energy milling and chemical synthesis techniques such as precipitation, alkoxides hydrolysis, sol-gel process, oxidation reduction and spark discharge methods. Each method has its own advantages and disadvantages but the main advantage of inert gas condensation method over any other method is the cleanliness of the system, minimum contamination of synthesized materials, flexibility in

controlling composition of evaporated material, flexibility of synthesizing multi component system and the use of reactive gases such as oxygen and hydrogen during evaporation in case of electron beam condensation process.

Inert gas condensation method can be scaled-up to produce large quantities of materials by increasing the size of the evaporation chamber and simultaneously evaporating many source materials. The cluster size in inert gas condensation can be controlled by controlling the evaporation rate and the inert gas pressure inside the evaporation chamber. It is reported in one of the study that the clusters with mean diameter as small as 3-4 nm have been synthesized by inert gas condensation (IGC) method.[6] Further, the same study showed that the purity level of the powders range from 10^{-2} at% oxygen for low oxygen affinity metals. The impurity level associated with IGC in the case of nickel is 0.2 at% hydrogen.[15] The oxygen content of materials with low oxygen affinity is on the order of one percent.[16] Baking of evaporation chamber walls can reduce the oxygen level to about 0.1%. Whereas the impurity level associated in case of mechanically alloyed (MA) NiAl is 0.63 at% oxygen and hydrogen[16] and 1-2 at% Fe.[17] Perhaps the only advantage associated with MA over IGC method is that much larger volumes of materials are produced.

In theory, IGC method is a process of evaporating materials in a vacuum chamber within which a hearth has been loaded with pre-cursor materials. These pre-cursor materials are heated and

evaporated with an electron beam. Before evaporation, the main chamber containing the pre-cursor material is sealed off from the turbo-molecular pumps and then back filled with an inert gas (such as helium, argon, or nitrogen) to a pressure of 0.2 - 0.3 torr. A super saturated region of atoms containing volatilized monomers is established above the pre-cursor source material during evaporation. These monomers aggregate into clusters by colliding with cold inert gas molecules. As a result of these collisions these monomers loose energy and form clusters. These clusters grow by adding monomers to individual clusters and by aggregation due to collision between clusters.[6] Since temperature reduced very quickly away from the pre-cursor source, therefore a large temperature gradient is established between source material and a liquid nitrogen filled cold finger served as a target for powder collection. As a result of this temperature gradient a convection current is established between source material and target cold finger. This convection current drives clusters towards cold finger where they adhere to the target surface by loosing its energy.

In case of IGC method, the mean cluster size can be controlled by controlling three parameters. These parameters include 1) temperature of the source material which in turn is related to the evaporation rate, 2) Pressure of the inert gas used during evaporation, 3) And the type of gas used. The temperature of the source material is determined by the dwell time of the electron beam on pre-cursor

material. The longer the dwell time the higher will be the temperature of the material which resulted in higher evaporation rate. As a result of higher evaporation rate, as partial pressure of metals reduces with increasing temperature, the concentration of atom in supersaturated regions will be much higher. Since the size of the cluster depends on time it spend above the supersaturated region, therefore convection current plays an important role in dictating its size. The convection current is directly proportional to the weight of the gas and the thermal gradient and inversely proportional to the pressure of the gas. Therefore higher the evaporation rate, the higher will be the temperature of the source material which in turn will increase the convection current. But at the same time a higher source temperature will increase the concentration of metal atoms in super saturated region which complicated the whole issue. The effect of metal vapor pressure and source temperature on the particle size can be seen in figure 3. On the other than the effect of the weight of the gas used and the pressure of the gas can be seen in figure 4.[4] From this figure it is clear that heavier inert gases and higher gas pressure can result in larger cluster size. Cluster formed in IGC apparatus exhibited a log normal size distribution.[6] The particle size distribution from IGC can be reduced by increasing the convection current. A fairly small particle size can be obtained in IGC by controlling source temperature, and the pressure of the inert gas.

Therefore in order to minimize the grain size, a slower evaporation rate along with lighter gas with low pressure is required.[18]

2.1.2. EXPERIMENTAL DETAILS:

The evaporation system used in this study to produce nanophase powders by well known gas condensation technique.[43,61] Nanocrystalline NiAl powder from precursor pre-cast NiAl and Nickel was synthesized by IGC process. The powders obtained by IGC method were thus used to produce all 9 mm disk shaped samples. The pre-cast NiAl (99.99%) used in the study was obtained from AEE (Atlantic Equipment Engineers). Also pure Ni pieces (99.99%) used in this study were obtained from Alfa AeSar. The as received NiAl was in the size range of about one to two inch pieces. In order to fit the Ni pieces into the hearth, used to collect pre-cursor material for evaporation, the material was cut down to about quarter inch pieces. Before evaporation these materials were cleaned ultrasonically for several hours in acetone to remove surface impurities, debris, and grease during cutting operation. Pre-cast NiAl pieces were loaded in the three hearths which were either lined with graphite liner for some evaporations or no loner was used for other evaporations. Pure Nickel pieces were loaded in fourth hearth which was always lined with graphite liner. The evaporation chamber was

cleaned thoroughly with alcohol and then with acetone to minimize any contamination from previous evaporations.

A schematic of the evaporation system is shown in figure 5. This system consists of three chambers; The main chamber, intermediate chamber, and gun chamber. Each chamber is hooked up to a turbo molecular pump. These three chambers are separated by Moly nozzles with 1.5 cm diameter whole in the middle. The function of the Moly nozzles is to guide the electron beam down to the source material and also to provide low conductance of gases between each chamber. The Electron gun which is a modified Pierce design,[19] is mounted at a 45 degree angle with respect to the main chamber. This gun is rated for continuous operation at up to 30 KV beam energy, and up to 200 mA beam current. After loading the material, the 30 inch diameter main chamber was sealed on the top with a Viton gasket. Then the chamber was evacuated using the mechanical roughing pump, that attained a vacuum of 60 - 70 torr, sorption pump that attained a vacuum of 0.01 - 0.1 torr and finally with turbo-molecular pumps. With the turbo molecular pumps the system was maintained under a vacuum of ~ 10^{-7} torr. In order to improve the vacuum further, the main chamber was baked with two high power lamps placed inside the chamber to drive off any trapped moisture, gases, and alcohol absorbed on the walls of the chamber. After overnight baking the baking lamps were turned off and the chamber was allowed to cool for about one hour. The average vacuum after cooling

of the chamber was between 1 ~ $5X10^{-7}$ torr. The pre-cursor material placed in four hearths were out gassed using low power Electron beam while maintaining temperature below the melting points of NiAl and Nickel. Out gassing of the precursor materials were typically carried out for about 5 ~ 10 minutes. During out gassing of pre-cursor material the main chamber was sealed off of the turbo pumps and the chamber was back filled with Helium gas to a pressure of around 0.2 ~ 0.3 torr. After out gassing the chamber was evacuated again by opening the gate valve to the turbo pump. Typically the evaporation chamber was flushed several times with Helium gas to a pressure of 0.2 - 0.3 torr before evaporation. A cold trap which is connected to the main chamber was filled with liquid nitrogen and allowed to cool down fully over the course of 30 to 40 minutes. The purpose of this cold trap is to further trap any moisture or gases present in the chamber. After all procedures the ultimate vacuum typically reached to low 10^{-7} to high 10^{-8} torr. Just before evaporation, the turbo pump to main chamber was sealed off again and the helium gas was bleeded into the main chamber with a bleeder valve. The helium gas pressure during evaporation was maintained between 0.2 ~ 0.6 torr.

Since Electron gun consists of a Tungsten filament, therefore a vacuum of 10^{-5} to 10^{-6} torr is required to generate an electron beam. Such a vacuum is needed to prevent the filament from rapid degradation. But on the other hand the evaporation inside the main chamber is carried out under a vacuum of 0.2 to 0.6 torr. In order to

obtain this pressure differential, the electron beam is allowed to pass through two molebdnium apertures. These apertures are 1.5 cm in diameter and 5 cm long. These apertures separate main chamber from intermediate chamber which in turn is separated from the gun chamber. Three pairs of electromagnetic lenses (one in each chamber) were used to focus and deflect the beam through these apertures and onto the desired position on the hearth. The gun region was pumped on with a 360 1/S turbo-molecular pump, an intermediate region was pumped on with a 2200 1/S turbo-molecular pump, and the main region which contained hearth and cold finger was pumped on with a 330 1/S turbo-molecular pump.[20] During evaporation the main chamber pump is valved off, while the two other chambers are pumped dynamically which maintained the gun region to a vacuum of ~ 10^{-6} torr.

A Helium gas pressure of 0.2 ~ 0.6 torr was used during evaporation inside the main chamber. An evaporation was started by energizing the electron gun with 30 KV. Initially a beam current of about 10 mA was applied and beam was focused on the hearth by varying the X, Y coordinates with the aid of a computer. After establishing all the targets, and after storing all target coordinates, the beam current was slowly increased to 90 to 120 mA. A cold finger was filled with liquid nitrogen prior to evaporation. The evaporated material condensed on cold finger during evaporation which was scrapped off continuously with three vertical scrappers rotating

slowly around the cold finger. The scrapped material was collected into a glass beaker placed directly underneath the cold finger. The helium gas pressure was monitored during evaporation using a pressure gauge. A variety of evaporation conditions were used to effect cluster size and NiAl powder yield. The various experimental conditions for evaporating NiAl powder are shown in table 1

The hearth region during evaporation can be seen in figure 6. This figure shows two materials evaporated simultaneously. Also an evaporant "plume" is clearly visible. The evaporation time varied from one to three hours depending on the conditions used and material collected. The electron beam was shut down after completing the evaporation. The helium gas valve was shut off, and turbo-molecular pump to main was opened to evacuate the chamber.

2.2 CONSOLIDATION:

2.2.1. INTRODUCTION:

Consolidation was carried out on powders produced by IGC method in order to obtain the required shape and green density.[2 1] Consolidation process resulted in the production of pellets, which are important from the point of view of mechanical behavior evaluation. Therefore in order to obtain pellets with higher green densities and

smaller number of flaws, defects, and contamination, a new consolidation system was designed and build. The new consolidation system is shown in figure 7. The samples produced by other investigators in the old compaction unit (figure 8) showed poorly compacted rim around the circumference of the samples.[22] In another investigation, nanophase Fe powder compacted in old compaction system also showed numerous radial cracks which were present in the lower compacted rim.[23]

A large portion of surface flaws can be removed by polishing the specimen. However the apparent tensile strength of nanophase Cu and nanophase Pd were highly dependent on these surface flaws.[24] Since old compaction system was not actively pumped during the final stage of consolidation, therefore the possibility of contamination such as oxidation was highly susceptible.

2.2.2. EXPERIMENTAL DETAILS:

During evaporation the powder collected on the cold finger was removed by three vertical stainless steel scrapers either continually or continuously. The scraped powder was collected into a glass beaker placed directly underneath the cold finger. The amount of powder collected in the glass beaker was monitored through a quartz window fitted on the small chamber which in turn is connected

to the main chamber and compaction unit simultaneously. The glass beaker was connected to a motion device, which was capable of transporting the evaporated powder through vacuum channel into the compaction unit. The motion device was capable of 360^{o} rotation to facilitate the powder to dump into the compaction die. The compaction unit and evaporation units were connected with 6 inch diameter channel separated by a hand operated gate valve. After the gate valve was opened between the compaction unit and the evaporation unit, the beaker was pushed into the compaction unit with the aid of said motion device. The position of the glass beaker, containing nanophase NiAl powder, in the compaction unit was monitored through a large quartz window located on the front of the compaction chamber.

The glass beaker was pushed such that it almost touch the upper piston. The compaction unit is fitted with a bake out lamp located at the rear of the unit. The powder, which was still in the beaker, was allowed to heat radiantly by the bake out lamp for few minutes. The removal of water vapors and trapped gases were monitored by the decrease in the vacuum in the compaction unit. The powder was dumped into a funnel attached to the die by rotating the motion device to 180^{o} clockwise. The function of this funnel was to direct the powder in to the center of the die. The empty beaker was pulled out of the compaction unit and gate valve between compaction unit and evaporation unit was closed. The powder which was stuck to the die

surface was pushed in the die by means of a vertical motion device fitted with flexible copper blades at the lower end. The motion device was plunged up and down by hand until most of the powder was pushed into the die. Once sufficient powder was dumped into the die, the top piston was released by loosing the clamp which held the piston up against the force of the vacuum. Some of the consolidations were done with die at 100 ^{o}C and some with die at temperatures ranging from 100 ^{o}C to 250 ^{o}C. The powder usually out gassed once it fell into a heated die. With the die less than 200 ^{o}C the powder usually did not out gassed so vigorously but with die temperatures above 200 ^{o}C the rapid out gassing also popped the powder out of the die. For consolidations above 200 ^{o}C, the die was initially held at 200 ^{o}C before powder dumping. After dumping, the die temperature was raised to desired level. Once the desired die temperature was achieved, the top piston was lowered down by the hydraulic pump at a slow rate to allow for the powder to distribute uniformly into the die. Once the pressure gauge started to rise above the zero load position and the powder began to resist the motion of the piston, the motion of the top piston was further reduced by closing the hydraulic flow control valve. Slow motion of the piston is necessary to avoid the compact from cracking and also to prevent the piston from breaking due to the bending stresses applied on the piston caused by the slight misalignment of the top piston with respect to the die and the bottom piston. The load was finally raised to 10.5 tons to yield a pressure of

1.4 GPA on the 9 mm diameter nanocrystalline NiAl compact. The additional load of 0.5 tons was used to compensate for the compression of the two springs used for retraction of the top piston from the die against the force of the friction, gravity and vacuum. The applied load was maintained at the desired temperature ranging from 60 minutes to 120 minutes. The prolonged holding ensured sintering and densification of nanocrystalline NiAl powder.

After the desired sintering time, the load was removed by slowly opening the hydraulic fluid return valve. After the load is removed the top piston is further raised about 1/2 inch while its lower end still remained inside the die. The lower piston was then completely removed out of the die by lowering it down with a hand operated winch. The compaction unit is hooked up with a sample removal system. It consists of a motion device with small glass crucible fitted to the end. It also consists of a quartz tube outside the main compaction chamber which is separated by a manually operated gate valve. This whole arrangement is also kept under vacuum. The glass crucible was pushed inside the compaction unit and aligned accurately with the die. This whole procedure can be easily monitored through a large quartz view port. The crucible which is directly underneath the die is ready to collect the specimen which is still inside the die. The specimen was pushed out of the die by lowering the top piston very slowly. A small view port was used to witness the specimen drop into the glass crucible. After the specimen

was dropped in to the glass crucible, it was pulled out of the compaction chamber using motion device. The gate valve to the quartz test tube was then opened and the specimen was dropped into the quartz test tube by rotating the motion device through 180^{o} either clockwise or counter clockwise. The gate valve which separates the quartz test tube was closed. The quartz test tube containing the specimen was still under vacuum. It can be either seated with oxy acetylene flame or the specimen can be removed by venting the test tube with either air or inert gas through a bleeder valve.

After the specimen was removed from the quartz test tube, it was evacuated again with a mechanical roughing pump and then with a turbo molecular pump. The gate valve was then opened between the test tube and the motion device. The bottom piston was pushed into the die and locked into position. The top piston was raised completely out of the die and was returned to its normal position with the help of compression springs located around the guideposts. The die temperature was brought down below 200 ^{o}C and the system was ready for subsequent consolidations. The temperature of the die was monitored by a K- type thermocouple. In order to ensure a good thermal contact of the thermocouple and the die, a screw with a large washer was used to push it against the die. The die was placed on a large aluminum block and was thermally separated from the aluminum block by a ceramic ring. The temperature of the aluminum block and guide posts were also monitored by thermocouple to ensure

that the temperature did not exceed 200 ^{o}C. The die temperature ranged from 25 ^{o}C to 400 ^{o}C, which was controlled by a precise temperature controller.

3. DENSITY MEASUREMENTS:

3.1. EXPERIMENTAL DETAILS:

The density of the compacted specimens were measured using the Archimedes principle. Measurements were made on 28 nanocrystalline specimens and a standard coarse grained NiAl specimen. A precision matler micro balance with a sensitivity of 10 μm was used for all measurements. The specimen dry weight was taken in the air first. Then each specimen was submersed in 1,1,1 Trichloroethane and was held for few minutes to completely wet the specimen surface. After weighing the specimen, it was then taken out of the 1,1,1 trichloroethane and allowed to evaporate excess surface liquid. The specimen was immediately weighed again in air. All measurements were taken twice in order to confirm the reliability of the data. The reliability of the measurements were turned out to be within 1% for all measurements on 28 nano crystalline NiAl samples. The densities of all specimens were reported in gm/cc and also as a function of standard density. NiAl has quite broad single phase region

with composition ranging from 45 to 59 at. % Ni (figure 9). The stoichiometric NiAl (49.9 at. % Al) has a density value of 5.85 gm/cc,[25] and the density increases steadily with increasing Ni content, but decreases as Ni is removed from the stoichiometric alloy.[26-29] The lattice constant of stoichiometric NiAl is 0.2887 ± 0.00001 nm,[26] which varies on either side of stoichiometric composition.[26,27,30-35] Figure 10 shows variation of lattice constant as a function of composition.[27] The density of non stoichiometric NiAl can be calculated based on the variation of lattice constant and is shown in figure 11.[36] Therefore the density of all specimens were corrected for non stoichiometric composition. The density of every specimen was calculated including open surface pores and excluding open surface pores by the following equations respectively.

$$D' = \frac{W_A(d-\rho)}{W_A - W_L} + \rho \qquad \text{.....(1)}$$

$$D' = \frac{W_A(d-2\rho)}{W_S - W_L} \qquad \text{.....(2)}$$

Where: D' = Sample density in gm/cc

d = Density of liquid (1,1,1, Trichloroethane, 1.309 gm/cc)

ρ = Density of air (0.0012 gm/cc)

W_A = Weight of the sample in air

W_L = Weight of the sample in liquid

W_S = Mass of the weight required to balance liquid saturated sample in air

3.2. **RESULTS:**

Results of all density measurements with corrected values for non stoichiometric composition are given in table 2. Density measurements were done on all specimens in as compacted state without any surface treatment. The as compacted specimens were produced in new compaction unit. All specimens compacted at temperatures ranging from 100 ^oC to 275 ^oC were found to have densities ranging from 78 to 92 % of the theoretical density. The mean value of 86.7 % of the theoretical density was found with a standard deviation of 3.4. The density measurement of coarse grained NiAl sample was determined to be 99.9 % of the theoretical density, indicating the precision of this method.

Figures 12(a & b) represent the as compacted densities of all specimens with compositions in the single phase region plotted against the grain size as determined by Scherrer formula (SF) and Warren Averbach (WA) single peak. It is evident from these figures that density increased with an increase in grain size, in general. Figure 13 showed the densities of as compacted specimens plotted against the bulk composition as determined by SEM, EDS analysis. The density increased with increasing Ni content, when more Nickel is added in

stoichiometric alloy, where as density decreased when Nickel is removed from the stoichiometric alloy. This trend is consistent with the literature for coarse grained NiAl.

Figure 14 showed density values plotted against die temperature during compaction. Specimens compacted at 100 ^{o}C show density values ranged from ~78 to 90 % of the theoretical, but specimens compacted at higher temperatures had density values well above 85 % of the theoretical with maximum value as high as 92 % of the theoretical.

4. CHARACTERIZATION:

4.1. XRD STUDIES:

4.1.1. INTRODUCTION:

The materials produced by inert gas condensation method have grain size in nanometer regime. Grain size of such bulk materials cannot be determined by conventional techniques, such as optical microscopy, SEM etc. Another approach to estimate grain size and grain size distribution in such materials is TEM analysis.[2,37-49] This method can be applied quite effectively on loose powders (unconsolidated). But such method is not very effective for bulk

specimens (consolidated), since it is a destructive process and requires thin foil which is not an easy task. Therefore X-ray diffraction is the only method which can be applied non destructively and quite efficiently. To obtain grain sizes in such materials X-ray diffraction (XRD) Scans of nanocrystalline NiAl compacts were done to estimate the presence of small grain size and strains present in the lattice. The correct knowledge of the grain size of nanocrystalline materials is very important, because mechanical properties of such materials are quite different and very much influenced by their small grain size. Therefore X-ray diffraction is a method of determining grain size by analyzing the shape and the breadth of the diffraction peaks. Such peak broadening could be due to the presence of very small grains, twins, dislocations, stacking faults, impurities, strain in the lattice, or instrumental broadening.

X-ray diffraction scans of materials with very small grain size showed an increase in peak broadening.[50-54] Cold working in a metal introduces dislocation substructure, in which such small angle grain boundaries which may broaden the peaks in XRD scan. The introduction of strain during cold or warm compaction and also strains associated with the formation of small particles may also broaden the peaks.[55]

The formation of multiply twins in FCC materials could also result in peak broadening.[22] A perfect crystal would still give some peak broadening due to instrumental effects such as; divergence of

the incident beam, slit width, dimensions of the specimen, the natural width of the X-ray lines themselves, imperfect focusing, and unresolved $\alpha_1 \& \alpha_2$ peaks.[50-54] In order to consider the peak broadening purely due to intrinsic effects such as grain size and strain, an allowance must be made for extrinsic effect such as instrumental broadening. Such instrumental broadening can be accounted for by running a standard peak in which particle size is large enough to eliminate broadening due to intrinsic effects. The standard scan can be subtracted from nanocrystalline NiAl scan to obtain broadening only due to particle size and strain in the lattice.

4.1.2. EXPERIMENTAL DETAILS:

X-ray diffraction scans for 28 nanocrystalline NiAl samples and one coarse grained NiAl standard (Obtained from Ames Laboratory) were obtained in $\theta - 2\theta$ scan mode. All scans were carefully analyzed to estimate grain size and the lattice distortion. Such estimates involved grain size determination by Scherrer method, Warren Avarbach double peak method and Nandi single peak method. (100), (110), and (211) peaks were used to estimate the grain size for Scherrer analysis. Higher order peaks were not chosen for this method because of background intensity present. Such background

levels can cause the peaks to broaden a lot which resulted in incorrect FWHM estimation.

All scans were done on Rigaku diffractometer with CuK_{α} radiation. Also Ni filter was used to reduce fluorescence. In order to be consistent, all scans were done with identical slits. An accelerating voltage of 30 KV and a current of 60 mA were used for all scans. The data was collected at the scan speed of 5^{o}/min. All samples were scanned from 20^{o} to 102^{o}, using 0.2^{o} to 0.05^{o} step size. In order to avoid any experimental error, each specimen was scanned twice with identical conditions.

After collecting XRD scans for all specimens, the data was converted into an ASCII file. For every specimens each peak was modeled using a computer program. Such modeling involved least squares fitting routine that used a Pseudo-Voigt profile for the model curve. In recent studies[58,59] Pseudo_Voigt function provide an excellent fit to broadened XRD scans. Fitted peaks were used to subtract the background intensity and to analyze the peak shape. The results obtained from computer analysis were used to obtain grain size based on Scherrer and Warren-Averbach method. Warren-Averbach double peak analysis was done on only few of the scans because of the low intensity and the poor statistics of (220) peak which resulted in difficulty in modeling such peak. Single peak method of Nandi et al.[60] was used on the (100), (110), (200), and (211) beaks to obtain grain size and lattice distortion.

4.1.3. **RESULTS:**

A representation XRD scan of nanocrystalline NiAl and coarse grained NiAl is shown in figure 15(a) & (b). Figure 16 shows XRD scan of nanocrystalline and coarse grain NiAl (110) peaks at around 2θ equals 44^{o}. The presence of small grain size and strain in the lattice in nanocrystalline NiAl can be seen by significant peak broadening. The peak fitted results of computer program for 14 specimens are shown in table 3. The data in table 3 included background intensity I_{bg}, maximum intensity I_o, fraction Lorentzian Vs Gaussian fit LG_f, Bragg angle $2\theta_B$, fwhm 2θ, and an estimate of the fitted profile. The fwhm values listed in table 3 are used to calculate the grain size by Scherrer method.

The XRD diffraction profiles obtained for nanocrystalline NiAl specimens had some differences among their data. These differences could be explained on the basis of compositional variation among various specimens. Also these differences could be explained due to the surface roughness, surface porosity, residual stresses, and the exact positioning of the small specimens in the X-ray beam. The ratio of the background value of the nanocrystalline samples to that of the standard coarse grained specimen is 1-2 on the average for the 100, 110, 200, Peaks and 2-4 for the 200 and 220 peaks. The profile intensity maximum (I_{max}) for the nanocrystalline samples as a fraction of I_{max} for the standard NiAl sample is 0.35 on average for

100 peak, 0.3 for 110 peak, and 0.5 for the 200 and 211 peaks. Also the fwhm value obtained for the 100 and 110 peaks were 2-3 times larger than the standard NiAl sample under same conditions.

4.1.4. **DISCUSSION:**

In order to estimate the grain size of nanocrystalline NiAl three different methods were used. These methods were based on Scherrer analysis, WA (Double Peak) using two orders of reflection, and Nandi single peak analysis. The results of grain size estimated by these three methods are shown in Table 4 & 5. Table 4 also showed ε_{rms} values obtained by single peak and double peak methods. The grain size obtained by all three methods were studied. Also comparison of the strains obtained by WA Double Peak Method and Nandi Single Peak method were studied. The correlation between grain size and strain was also studied.

The grain size estimates of all nanocrystalline samples determined by the WA double peak method and Nandi single peak method usually agree to within 24 % on average. For 8 samples the difference in grain size estimate is less than 10 % obtained by these two methods, the difference in the grain size estimate is less with smaller grain size. The difference in the ε_{rms} estimated by the two methods is 50 %. For sample with their ε_{rms} values not very much

different (within 20 %) calculated by WA double peak method and Nandi Single Peak method did not show significant differences in their grain size. The ε_{rms} values obtained by double peak method on the average for all specimens were almost half that of single peak values.

The grain size obtained by Scherrer method is usually larger by a factor of 1-3 on average than the WA method. Since the volume averaged Scherrer method weighs larger grain sizes more heavily than the area averaged WA method, therefore it means that the differences in the two results could be due to the presence of some volume fraction of larger grains than the average grain size in these samples.

From the above study it is clear that the grain size and lattice strains obtained for different specimens showed significant variation from sample to sample. This is regardless of the fact that all specimens were prepared under nearly identical conditions i.e. almost identical beam currents, grid voltage, and He gas pressure. Then all samples were consolidation to a 9 mm palette at 1.4 GPA pressure under high vacuum conditions at die temperature ranging from 100 to 250 ^{o}C. The above variation in the grain size and lattice strain could be explained due to the variability in the processing parameters and uncertainties associated with measurements.

Although the processing conditions were apparently identical from sample to sample, small, non symmetric variations in evaporation rate, beam current, beam intensity and He gas pressure

are likely to have occurred during the evaporation process. First of all there is no way of monitoring the temperature of the source material, since evaporation rate depends strongly upon the instantaneous temperature of the source material. A slight variation in the temperature could result in variable evaporation rate which will in turn result in a variation in grain size. The evaporation rate is proportional to electron beam power, which is a function of Accelerating voltage i.e. 30 KV and beam current which can be set anywhere between 1 to 200 mA. A slight variation in the accelerating voltage or beam power could result in variation in beam power, which in turn lead to a variation in evaporation rate with the consequence of variation in grain size. Also the electron beam passed through apertures and nozzles before it finally reach the source material. The path of the beam and focusing is done by sets of variable deflection and focusing electro-magnetic coils. The path of the beam is constantly adjusted by controlling these electro magnetic coils during evaporation. A slight deviation of the beam from its path or slight defocusing of the beam could result in a loss of beam out put power despite the fact that almost similar beam current and accelerating voltage were used. Furthermore, variations in the pressure of the He gas used during the evaporation also could result in grain size variation. Therefore for samples obtained under similar conditions, the variation observed in grain size could be due to the fluctuations in

beam power, evaporation rate, temperature of source material and gas pressure during evaporation.

The second source of variation in grain size and lattice strain associated with samples obtained under similar conditions are due to the uncertainties in the analytical precision of the XRD procedures. Since the broadening of diffraction profile is a function of grain size, lattice strain, and instrumental broadening, therefore a slight variation in estimating either one of these will result in errors in accurately measuring the grain size and lattice strain. Accurate measurement of area under the diffraction profile for either single peak or two orders of peaks is necessary to obtain good estimates of the broadening. Since the Scherrer method is based on FWHM (Full width at half maximum), therefore accurate removal of background intensities from peak profile is necessary. Instrumental broadening effect may not be removed quite successfully from sample to sample due to the variation in the sample size, surface roughness, ,surface impurities. The variation of grain size and lattice strain within the specimen could effect the accuracy with which one is able to de-convolute grain size, strain, and instrumental broadening. Since the diffraction profile averages over all the variations present on the specimen surface, therefore the variation of surface strains, impurity concentration, and surface roughness could result in inaccuracies associated from sample to sample. Errors in grain size estimate obtained by Scherrer method for sample made under similar

conditions are estimated to be on the order of 50 - 100 %. The error associated with grain size estimate obtained by WA method for similar specimens are on the order of 100 - 150 %. It is clear from equation 3 (below) that similar errors must be present in the lattice strain estimates.

$$A_{L(hkl)} = A_S^L(hkl)A_D^L(hkl) \quad \text{.....(3)}$$

Where $A_{L(hkl)}$= Fourier cosine coefficient for reflection hkl (hkl are miller indices of diffracting plane)

$A_S^L(hkl)$= Particle size coefficient at a given scattering column length (L), independent of line order n

$A_D^L(hkl)$= Strain coefficient at a given L, dependent of line order n

4.2 SEM AND OPTICAL MICROSCOPY:

4.2.1. INTRODUCTION:

Scanning electron microscopy was performed on as-consolidated as well as polished nanocrystalline NiAl samples. Such analysis were done to develop an insight about the surface structure

features, such as deflects, cracks, inhomogenity, porosity, and surface Finnish. Such tests were also done to determine the overall quality of the specimens, which is very important in determining the mechanical properties. The resolution provided by the SEM was good enough to establish such conclusions. SEM and optical microscopy was performed to determine how homogenous is the area under investigation. Information about the material flow during consolidation can also be deduced from such SEM and optical analysis. SEM study can also reveal the pore size, pore density, and pore size distribution in the scanned area. SEM analysis was also performed to reveal the effect of consolidation temperatures on factors such as: material flow during consolidation, the amount of porosity and pore size distribution. Optical microscopy can reveal facts such as uniformity of the surface, surface contamination, and the presence of cracks. Information about surface impurities can also be obtained from SEM analysis.

The samples produced by the old compaction unit showed regions of gross porosity and a region of low compacted material around the outer rim of the specimens[22,23] which can be seen in figure 17. The low compaction rim formed in specimens compacted in old compaction unit was probably due to the application of low pressure with a laboratory mechanical jack followed by the application of load of 10 tons under a hydraulic press. Between the application of small pressure and large hydraulic pressure, the whole

compaction chamber along with the loosely compacted powder was transported from the IGC main chamber to the hydraulic press. The removal of the old compaction chamber from IGC unit sometimes required shaking, tapping and jerking. The presence of the low compacted rim and gross porosity could have happened due to the reasons discussed above in addition to the crude control of load application and removal during both stages of consolidation. One of the functions of the SEM and optical microscopy analysis was also to verify the fact that either of those (gross porosity and presence of low compacted material) problems were removed in specimens consolidated in new compaction unit. The new consolidation unit was designed to eliminate such defects and problems associated with handling. In the new consolidation unit the load is applied by a hydraulic ram which can apply load at a very controlled rate. Such controlled application of load may help in breaking up agglomerates and provide more uniform distribution of material which help to reduce the pores. The die in the new consolidation unit can also be heated to 400 ^{o}C in a controlled manner which may further help the material to flow more uniformly. The load was removed in a controlled manner which further reduced the number of delimitation cracks.

SEM used in this study was fitted with an energy dispersive spectroscopic (EDS) detector. EDS analysis was done on as-consolidated as well as polished specimens at low magnification to determine the

overall chemical composition and also to determine the chemical homogeneity through out the compacted specimen.

4.2.3. **RESULTS:**

All samples of nanocrystalline NiAl were produced in new consolidation unit. All specimens were compacted at temperatures ranging from 100 ^{o}C to 275 ^{o}C. Figure 18 shows optical photo micrograph of warm consolidated nanocrystalline NiAl produced in new consolidation unit. There is no evidence of any large regions of porosity or the presence of low compacted rim. Several specimens viewed under low magnification did not show significant cracks present on the surface. Few specimens showed some cracks near the circumference which can be seen in figure 19 (a) and (b). Such cracks have no regular pattern and they were randomly oriented. Such cracks may resulted during removal of the load and/or during extraction of the specimen from the die. These cracks could also originate during handling and experimentation.

Most of the specimens appeared to be uniformly dense across the consolidation surface. Some specimens showed surface contamination which were consolidated at higher temperature (> 200 ^{o}C). Such contamination was found to be, which can be seen in fig 20, Tungsten Carbide (WC) which was also confirmed by XRD analysis.

Such confirmation occurred due to the reaction at the piston surface. Such contamination was only few μm deep and completely eliminated during polishing. All specimen surfaces were quite shiny and metallic in appearance in the as-consolidated state.

Few specimens showed "string like" features with random orientation in as consolidated state, which can be seen in figure 21. These strings were 1-2 μm in width on average. Figure 22 is an SEM photo micrograph of polished specimen, compacted at 100 ^{o}C, taken at high magnification to reveal the presence and nature of voids and defects present. By examining this figure it is clear that pore size ranged from 1-2 μm on average. Majority of the pores connected to one another to form lanticular type features.

5. SUMMARY:

This research was conducted to study the processing, characterization, and properties of single phase nanocrystalline NiAl. The principal results of the study are:

1) Nanocrystalline NiAl samples have been produced successfully by inert sag condensation (IGC) process. All samples were synthesized in helium atmosphere by evaporating pre-cast NiAl as a source material. All samples were compacted in the new consolidation unit under warm consolidation conditions. All consolidations were done

under high vacuum condition to minimize contamination and oxidation of synthesized powder.

2) The density of all samples were measured by Archimedes principal. As-consolidated nanocrystalline NiAl samples showed density values ranging from 75% to 95% of the theoretical.

3) X-ray diffraction line broadening method was used to estimate the grain size and long range lattice strain in as-consolidated samples. The average grain size estimated by Scherrer method and Warren Averbach (WA) method ranged from 2 to 10 nm for all samples in as-consolidated state. Lattice strain obtained by WA method ranged from $1\text{-}8\text{x}10^{-3}$ for all samples.

4) EDS analysis of all samples showed chemical composition well within the single phase region of NiAl. SEM and optical microscopy did not show regions of gross porosity or radial cracks in most of the samples. Few samples showed cracks near the edge of the sample that may have been caused during specimen removal from the die. All samples appeared to be uniformly dense and shiny in appearance. Few samples showed "string like" features of about 1-2 μm in width that may have caused during projection of agglomerates during consolidation.

Table 1 *Experimental conditions used to synthesize nanocrystalline NiAl powder byIGC method in the presence of ultra high purity argon gas.*

SPECIMEN #	# OF HEARTHS FOR NiAl	# OF HEARTHS FOR Ni	TOTAL # OF BEAMS ON NiAl	TOTAL # OF BEAMS ON Ni	GRAPHITE HEARTH LINER
I	3	1	8	1	YES
J	3	1	8	1	YES
K	3	1	8	1	YES
L	3	1	8	1	YES
M	3	1	8	1	YES
N	3	1	8	1	YES
O	3	1	8	1	ONLY NI
P	3	1	8	1	ONLY NI
Q	3	1	8	1	ONLY NI
R	3	1	8	1	ONLY NI
S	3	1	8	1	ONLY NI
T	3	1	8	1	ONLY NI
U	3	1	8	1	ONLY NI
V	3	1	8	1	ONLY NI

Table 1 *(Contd.)*

SPECIMEN #	NI DWELL TIME (ms)	NIAL DWELL TIME (ms)	DELAYED TIME (ms)	VACUUM Torr	HELIUM PRESSURE (Torr)	BEAM CURRENT (mA)
I	10	10	100	$4x10^{-7}$	0.3	110
J	10	10	100	$3.5x10^{-7}$	0.3	100
K	10	10	150	$1.5x10^{-7}$	0.3	110
L	10	10	150	$1.9x10^{-7}$	0.3	110
M	10	10	150	$9.5x10^{-8}$	0.3	110
N	10	10	200	$1.1x10^{-7}$	0.3	110
O	10	10	200	$6.6x10^{-7}$	0.3	110
P	10	5	300	$2.5x10^{-7}$	0.3	110
Q	5	5	600	$1.2x10^{-7}$	0.3	110
R	10	10	100	$2.0x10^{-7}$	0.3	90
S	10	10	100	$5.2x10^{-7}$	0.3	100
T	10	10	100	$9.8x10^{-8}$	0.4	100
U	10	10	100	$1.2x10^{-7}$	0.5	100
V	10	10	100	$9.0x10^{-8}$	0.6	110

Table 1 *(Contd.)*

SPECIMEN #	# OF HEARTHS FOR NiAl	# OF HEARTHS FOR Ni	TOTAL # OF BEAMS ON NiAl	TOTAL # OF BEAMS ON Ni	GRAPHITE HEARTH LINER
W	3	1	6	1	YES
X	3	1	8	1	YES
Y	3	1	8	1	YES
Z	3	1	8	1	YES
A1	3	1	6	0	YES
A2	3	1	8	1	ONLY NI
A3	3	1	8	1	ONLY NI
A4	3	1	8	1	ONLY NI
A5	3	1	8	1	ONLY NI
A6	3	1	8	1	ONLY NI
A7	3	1	8	1	ONLY NI
A8	3	1	8	1	ONLY NI
A9	3	1	8	1	ONLY NI
A10	3	1	8	1	ONLY NI
A11	3	1	8	1	ONLY NI
A12	3	1	8	1	ONLY NI

Table 1 *(Contd.)*

SPECIMEN #	NI DWELL TIME (ms)	NIAL DWELL TIME (ms)	DELAYED TIME (ms)	VACUUM torr	HELIUM PRESSURE (Torr)	BEAM CURRENT (mA)
W	13	10	150	3.8×10^{-7}	0.3	100
X	11	10	150	1.8×10^{-7}	0.3	100
Y	10	10	150	1.7×10^{-7}	0.3	105
Z	10	10	150	5.8×10^{-8}	0.3	110
A1	0	10	150	9.2×10^{-8}	0.3	105
A2	12	10	100	3.8×10^{-7}	0.3	115
A3	12	10	100	2.1×10^{-7}	0.3	117
A4	10	10	100	1.0×10^{-7}	0.3	115
A5	10	10	100	1.2×10^{-7}	0.3	115
Á6	12	10	100	7.0×10^{-7}	0.3	120
A7	10	10	100	1.8×10^{-7}	0.3	115
A8	10	10	100	1.1×10^{-6}	0.3	120
A9	10	10	100	2.0×10^{-7}	0.3	105
A10	10	10	100	1.9×10^{-7}	0.3	115
A11	10	10	100	1.3×10^{-7}	0.3	110
A12	10	10	100	1.1×10^{-7}	0.3	115

Table 2 *Summary of density values for all nanocrystalline NiAl specimens in the as-consolidated state including and excluding open surface pores, also include values corrected density values for non-stoichiometric composition*

Sample	Density Incl. Open Pores	Density Excl. Open Pores	Corrected Density for Composition	Density (% Theoretical)
I	4.48	4.49	5.01	89.57
J	5.49	5.50	6.99	78.72
K	4.50	4.51	5.34	84.42
L	4.33	4.35	5.39	80.72
M	4.61	4.64	5.53	83.90
N	4.71	4.74	5.46	86.75
O	4.97	4.98	6.09	81.72
P	4.71	4.72	5.66	83.37
Q	4.58	4.61	5.22	88.32
R	4.65	4.66	5.18	89.92
S	4.58	4.59	5.22	87.93
T	4.72	7.73	5.59	84.67
U	4.76	4.78	5.57	85.85
V	4.85	4.85	5.44	89.22
W	4.02	4.02	4.63	86.65
X	4.32	4.32	5.11	84.59
Y	4.38	4.39	5.01	87.37
Z	4.35	4.35	5.02	86.61
A1	4.43	4.43	5.05	87.51
A2	4.04	4.04	4.49	90.05
A3	4.44	4.44	5.12	86.78
A4	4.56	4.56	5.08	87.23
A5	-	-	-	-
A6	-	-	-	-
A7	4.04	4.04	4.32	93.58
A8	4.66	4.66	5.28	88.13
A9	-	-	-	-
A10	4.50	4.50	4.92	91.48
A11	4.72	4.72	5.16	91.22

Table 3 *Summary of the data obtained from the Pseudo-Vigot procedure for 14 XRD scans of nanocrystalline NiAl as-compacted samples.*

Specimen	File #	Peak	I_0	LG_f	$2\Theta_B$	fwhm	Quality
NiAl-I	2661	100	34.5	0.8960	31.21	1.0951	0.3008
NiAl-I	2662	110	289.8	0.8120	44.63	1.4900	0.4830
NiAl-I	2663	200	20.4	1.5000	64.91	2.0702	0.6374
NiAl-I	2664	211	47.7	1.0595	82.12	2.1837	0.4560
NiAl-I	2665	220	9.2	1.0000	98.99	0.818	0.5221
NiAl-J	2671	100	20.0	1.0000	30.98	0.5566	0.6198
NiAl-J	2672	110	298.2	0.6929	44.49	2.1000	0.6198
NiAl-J	2673	200	15.0	0.9422	65.09	2.5000	0.6761
NiAl-J	2674	211	22.3	0.1981	82.19	2.7498	0.7511
NiAl-J	2675	220	11.6	1.0000	98.80	0.4636	0.6473
NiAl-K	2681	100	19.3	0.5286	31.51	1.4598	0.4728
NiAl-K	2682	110	234.4	0.6722	44.70	1.7335	0.4728
NiAl-K	2683	200	24.6	1.0000	65.06	1.7488	0.5449
NiAl-K	2684	211	45.9	0.9471	82.25	2.3764	0.4287
NiAl-K	2685	220	9.6	0.5868	98.78	0.5868	0.8697

Table 3 *(Contd.)*

Specimen	File #	Peak	I_0	LG_f	$2\Theta_B$	fwhm	Quality
NIAL-L	2691	100	27.4	0.6430	31.33	1.6604	0.4768
NiAl-L	2692	110	243.7	0.7170	44.67	1.7061	0.5243
NiAl-L	2693	200	23.5	1.0000	65.06	2.0565	0.4309
NiAl-L	2694	211	44.2	0.9228	82.18	1.2866	0.5482
NiAl-L	2695	220	10.0	1.0000	98.42	1.3891	0.3456
NiAl-M	2701	100	54.4	0.5085	31.13	1.6341	0.7035
NiAl-M	2702	110	530.9	0.8105	44.56	1.6492	0.4173
NiAl-M	2703	200	42.6	1.1194	65.00	2.1590	0.4446
NiAl-M	2704	211	70.0	0.8311	82.10	2.5958	0.3913
NiAl-M	2705	220	14.3	1.0000	98.66	1.7009	0.5337
NiAl-N	2731	100	38.8	0.7273	31.41	1.5472	0.4534
NiAl-N	2732	110	488.8	0.7734	44.56	1.785	0.6368
NiAl-N	2733	200	24.1	0.9247	64.97	2.0851	0.5051
NiAl-N	2734	211	41.9	1.0000	82.11	2.9486	0.9941
NiAl-N	2735	220	12.2	0.6889	98.10	1.8773	0.8042
NiAl-O	2741	100	34.5	1.0000	31.43	1.3083	0.9393
NiAl-O	2742	110	501.2	0.7192	44.45	1.7833	0.6468
NiAl-O	2743	200	29.9	0.7437	65.01	1.9345	0.4708
NiAl-O	2744	211	38.1	0.4764	82.01	2.3248	0.9378

Table 3 *(Contd.)*

Specimen	File #	Peak	I_0	LG_f	$2\Theta_B$	fwhm	Quality
NiAl-P	2751	100	41.0	1.0000	31.01	1.5174	0.5850
NiAl-P	2752	110	450.4	0.6792	44.50	2.0259	0.4965
NiAl-P	2753	200	28.1	0.0779	65.05	2.3274	0.4916
NiAl-P	2754	211	45.7	0.6673	82.16	3.0572	0.4671
NiAl-P	2755	220	98.06	0.3900	98.06	3.2521	0.7389
NiAl-Q	2761	100	46.5	0.5204	31.05	1.6147	0.5011
NiAl-Q	2762	110	536.00	0.7581	44.51	1.6676	0.4557
NiAl-Q	2763	200	30.5	0.6556	64.75	2.4233	0.7578
NiAl-Q	2764	211	63.1	0.4610	82.11	3.0575	0.4589
NiAl-Q	2765	220	14.4	1.0000	98.37	1.8664	0.2358
NiAl-R	2901	100	19.3	1.0000	31.60	0.9082	0.9029
NiAl-R	2902	110	348.7	0.6115	44.42	2.2054	0.5323
NiAl-R	2903	200	20.5	1.0000	65.11	1.9232	0.4663
NiAl-R	2904	211	21.9	0.7191	81.96	2.0932	1.1732
NiAl-R	2905	220	3.6	0.2924	97.44	1.4446	0.7286
NiAl-S	2911	100	41.1	1.0000	31.11	1.3901	0.9762
NiAl-S	2912	110	419.7	0.6599	44.67	1.8097	0.5984
NiAl-S	2913	200	28.7	0.7429	65.12	2.4996	0.7329
NiAl-S	2914	211	38.7	1.0000	82.28	3.4107	0.8777

Table 3 *(Contd.)*

Specimen	File #	Peak	I_0	LG_f	$2\Theta_B$	fwhm	Quality
NiAl-S	2915	220	9.9	1.0000	98.19	0.6641	0.9006
NiAl-T	2921	100	60.5	0.8201	31.15	1.5167	0.4496
NiAl-T	2922	110	619.1	0.9834	44.55	1.4302	0.4142
NiAl-T	2923	200	40.6	1.2094	64.96	2.1498	0.6250
NiAl-T	2924	211	63.2	1.0000	81.98	2.5666	0.6985
NiAl-T	2925	220	18.9	1.4318	98.42	1.1900	0.5114
NiAl-U	2931	100	50.5	0.8963	31.06	1.2477	0.6343
NiAl-U	2932	110	504.2	0.9855	44.46	1.4249	0.4515
NiAl-U	2933	200	32.1	1.0798	64.76	1.7883	0.6453
NiAl-U	2934	211	55.6	0.8054	81.95	2.8012	0.5874
NiAl-U	2935	220	6.9	1.0000	98.00	0.9227	0.9027
NiAl-V	2941	100	45.7	0.7614	31.03	1.4601	0.4485
NiAl-V	2942	110	461.00	0.9277	44.58	1.7591	0.8199
NiAl-V	2943	200	28.3	1.2572	64.83	1.8872	0.7174
NiAl-V	2944	211	54.1	0.7616	82.20	2.5272	0.4987
NiAl-V	2945	220	8.9	1.0000	98.77	0.6045	0.7965

Table 4 *Summary of grain size estimates, calculated by Scherrer method, based on fwhm of (100), (110), and (211) peaks*

Sample	Grain Size nm			
	(100)	(110)	(211)	Mean
NIAL-I	10.072	6.369	5.805	7.415
NIAL-J	-	4.289	4.274	4.279
NIAL-K	6.524	5.325	5.164	5.671
NIAL-L	5.530	5.423	5.441	5.465
NIAL-M	5.638	5.640	4.593	5.290
NIAL-N	6.045	5.146	3.923	5.038
NIAL-O	7.590	5.150	5.310	6.017
NIAL-P	6.193	4.472	5.227	5.297
NIAL-Q	5.722	5.566	3.756	5.015
NIAL-R	15.153	4.064	6.171	8.463
NIAL-S	6.963	5.068	3.311	5.114
NIAL-T	6.199	6.696	4.656	5.850
NIAL-U	8.134	6.724	4.170	6.343
NIAL-V	6.514	5.234	1.957	4.568
NIAL-W	4.444	4.194	3.117	3.918
NIAL-X	4.416	6.119	5.524	5.350
NIAL-Y	8.001	6.416	5.362	6.594
NIAL-Z	6.558	5.291	4.197	5.348

Table 4 *(Contd.)*

Sample	Grain Size nm			
	(100)	(110)	(211)	Mean
NIAL-A1	7.394	5.341	4.055	5.594
NIAL-A2	7.257	5.972	5.287	6.172
NIAL-A3	8.269	5.544	4.349	6.054
NIAL-A4	15.128	5.675	5.327	8.707
NIAL-A6	5.368	5.887	6.394	5.883
NIAL-A7	19.625	7.392	6.248	11.080
NIAL-A8	6.968	6.674	7.659	7.100
NIAL-A9	15.582	6.487	5.280	9.110
NIAL-A10	8.918	6.870	7.431	7.739
NIAL-A11	-	6.232	4.789	3.671
NIAL-A12	8.598	7.225	5.650	7.157

Table 5 *Summary of Grain size calculations based on Nandi single peak method and Warren-Averbach double peak method. All values are based on as-consolidated specimens. Also shown are calculated mean long range strains($<\varepsilon 10^2>^{1/2}$), calculated at 50 ^{0}A scattering length for single peak and double peak XRD data.*

Sample	Single Peak					Double Peak			
	(100)	(110)	(211)	Mean	ε_{rms} (10^{-3})	(100)(200)	(110)(220)	Mean	ε_{rms} (10^{-3})
NIAL-I	2.7	2.9	3.0	2.9	9.4	2.9	-	2.9	6.1
NIAL-J	3.2	1.9	4.0	3.0	9.2	-	1.3	1.3	7.5
NIAL-K	3.4	2.7	2.4	2.8	8.9	-	-	-	-
NIAL-L	2.1	2.7	2.2	2.3	11.2	-	-	-	-
NIAL-M	2.4	2.5	2.1	2.3	10.3	-	-	-	-
NIAL-N	2.8	2.6	2.3	2.6	10.3	2.6	2.3	2.45	-
NIAL-O	2.6	2.5	2.8	2.6	10.6	2.2	-	2.2	-
NIAL-P	2.1	2.2	2.2	2.2	11.5	2.2	1.7	1.95	-
NIAL-Q	2.9	2.8	2.3	2.7	9.9	2.6	-	2.6	-
NIAL-R	2.7	1.9	4.6	2.2	9.8	2.4	1.5	1.95	-
NIAL-S	3.3	2.6	2.1	2.7	9.3	3.4	2.4	2.9	-
NIAL-T	3.2	3.0	2.1	2.8	9.4	3.4	2.5	2.95	4.3
NIAL-U	2.9	2.7	2.1	2.6	10.3	2.7	2.2	2.45	-
NIAL-V	3.3	2.6	2.4	2.8	9.3	3.2	2.2	2.7	3.7
NIAL-W	2.2	1.9	2.1	2.1	10.9	2.1	1.7	1.9	-
NIAL-X	3.5	2.6	2.5	2.9	6.9	3.3	2.7	3.0	3.1
NIAL-Y	4.2	3.2	2.4	3.3	6.2	4.2	2.3	3.25	1.0
NIAL-Z	3.0	2.7	2.2	2.6	8.0	2.6	2.8	2.7	-

Table 5 *(Contd.)*

Sample	Single Peak					Double Peak			
	(100)	(110)	(211)	Mean	ε_{rms} (10^{-3})	(100)(200)	(110)(220)	Mean	ε_{rms} (10^{-3})
NIAL-A1	3.0	2.5	1.8	2.4	9.0	2.8	2.2	2.5	-
NIAL-A2	3.8	2.8	2.5	3.0	8.1	3.9	-	3.9	3.5
NIAL-A3	3.0	2.9	2.2	2.7	7.8	2.9	3.0	2.95	3.4
NIAL-A4	3.3	3.0	2.5	2.9	6.9	3.1	2.9	3.0	-
NIAL-A5	2.0	2.8	2.8	2.5	9.4	1.7	3.3	2.5	4.9
NIAL-A6	14.6	3.4	4.5	7.5	3.4	-	2.7	2.7	4.5
NIAL-A7	-	3.4	3.1	3.2	8.4	-	3.8	3.8	4.1
NIAL-A8	3.2	3.5	2.5	3.1	6.6	2.9	3.6	3.25	2.3
NIAL-A9	5.1	3.3	3.6	4.0	4.9	4.4	3.1	3.75	-
NIAL-A10	4.6	3.2	2.6	3.5	5.7	4.8	2.9	3.85	3.5
NIAL-A11	4.5	4.6	3.1	4.1	4.8	3.8	5.5	4.65	4.3

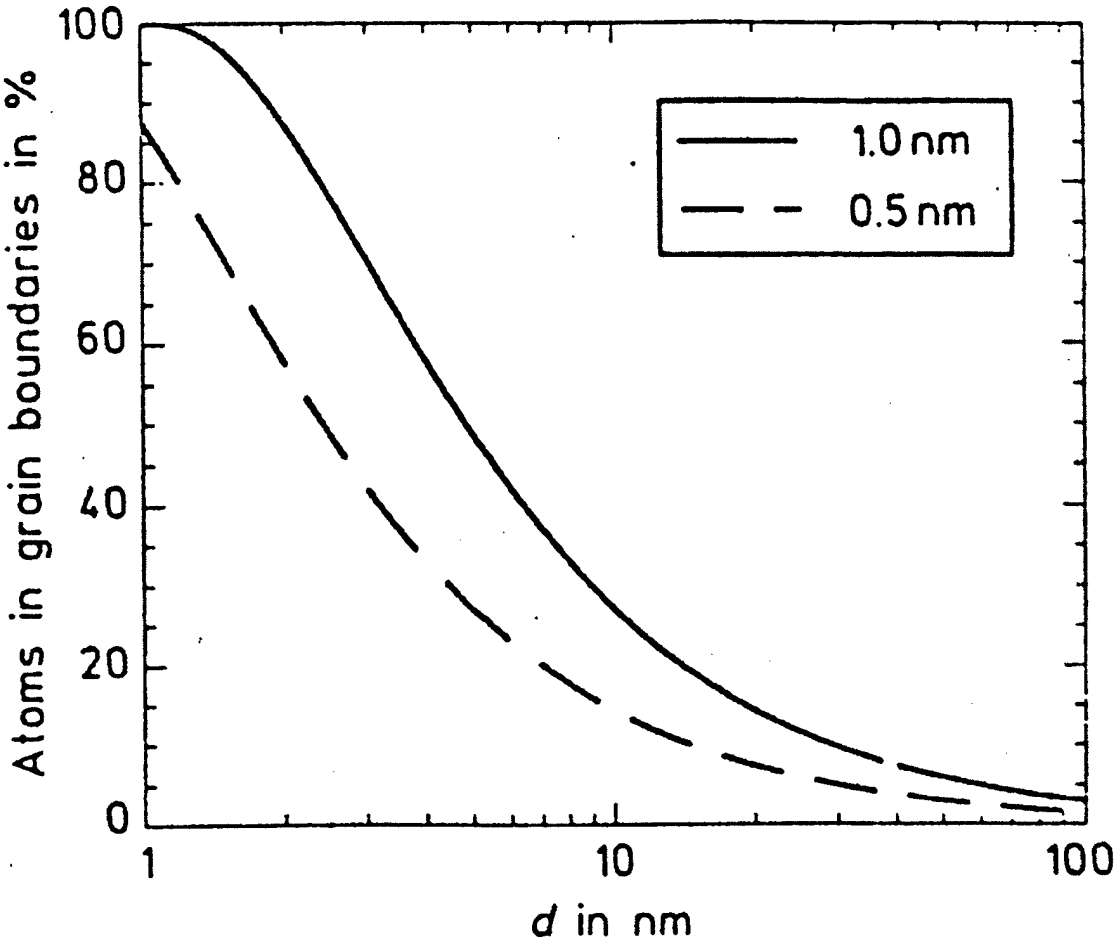

Figure 1 Figure shows percentage of atoms in the grain boundaries as a function of grain diameter, assuming grain boundary thickness varies from 0.5 to 1.0 nm. (Siegel 1991)

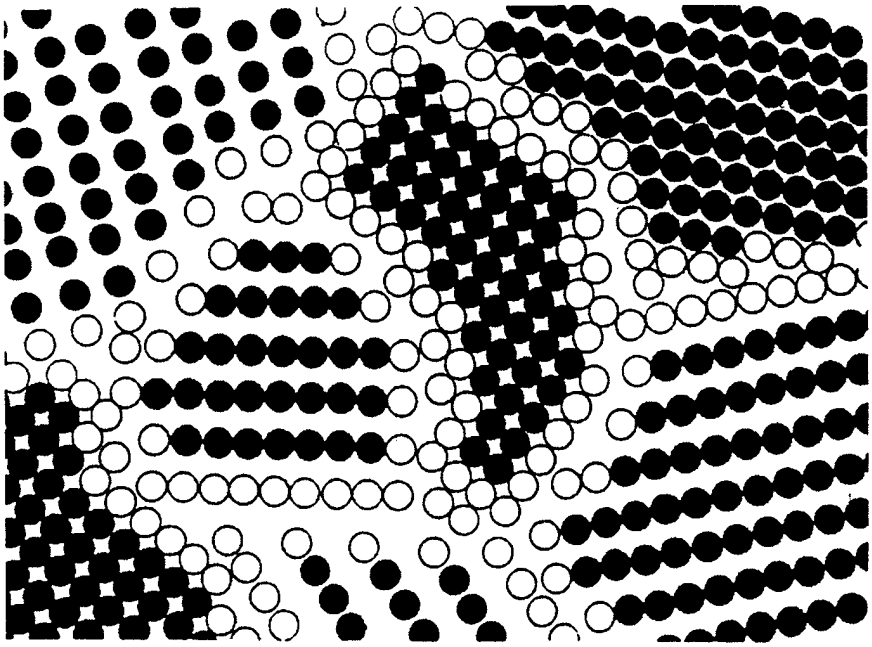

Figure 2 Schematic representation of a nanocrystalline material shows atoms associated with crystalline component (full circles) and thoseassociatedwith grain boundary network (open circles)

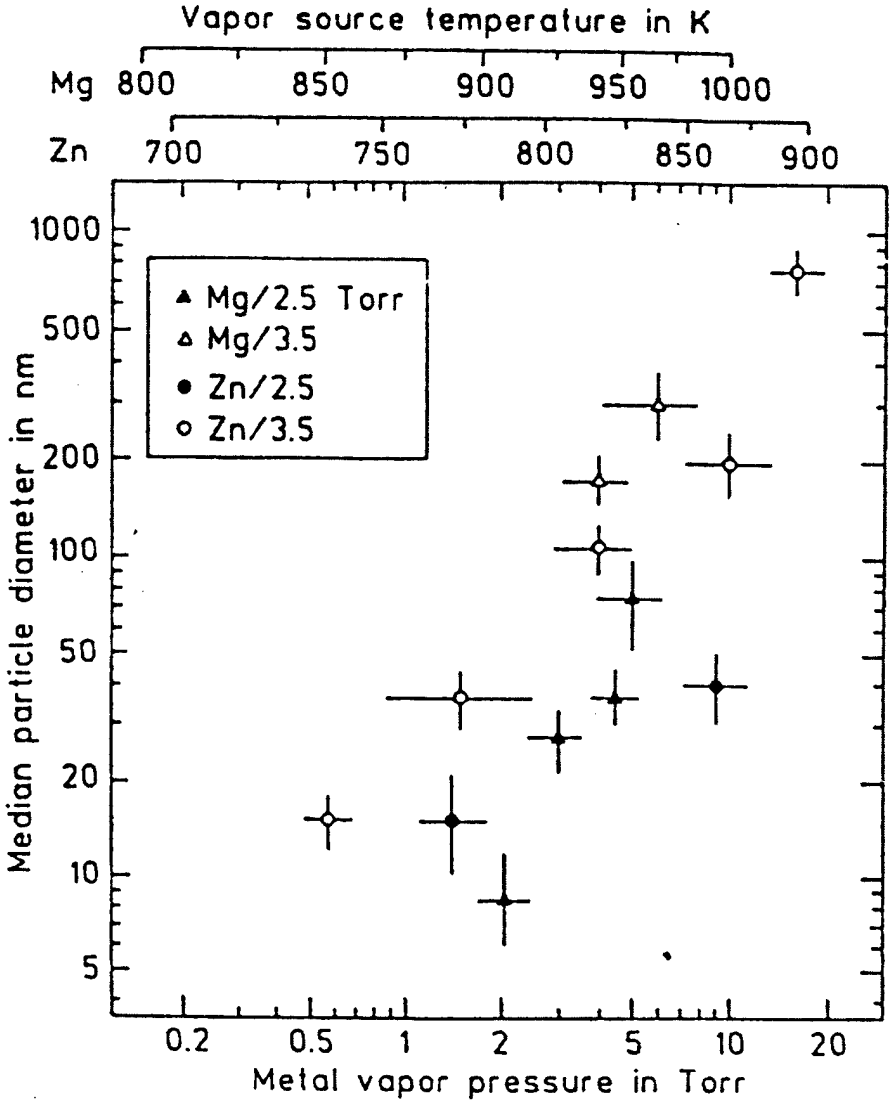

Figure 3 Figure shows median particle diameter versus vapor pressure at the metal surface (or the source temperature) for Mg and Zn evaporated and gas-condensed in two different Ar pressures. (Granquvist and Buhrman 1976)

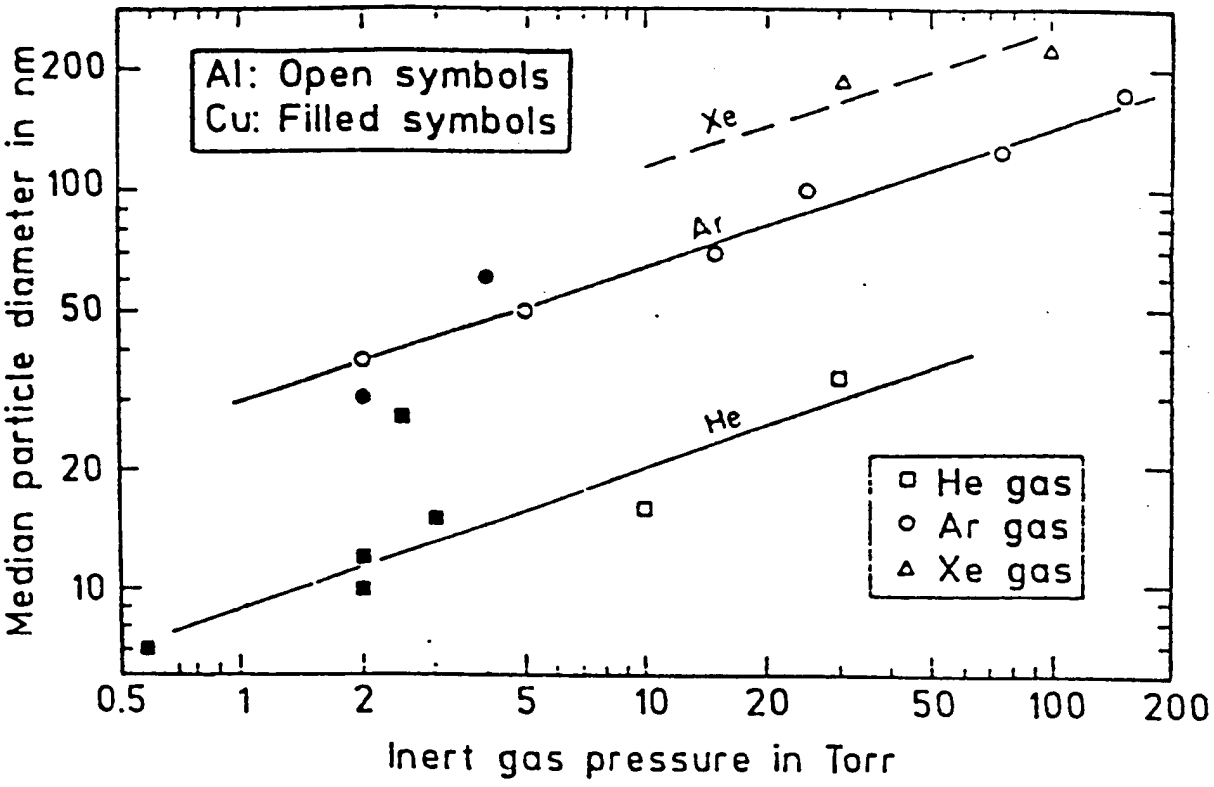

Figure 4 Effect of gas pressure and type of gas used during evaporation on the particle size

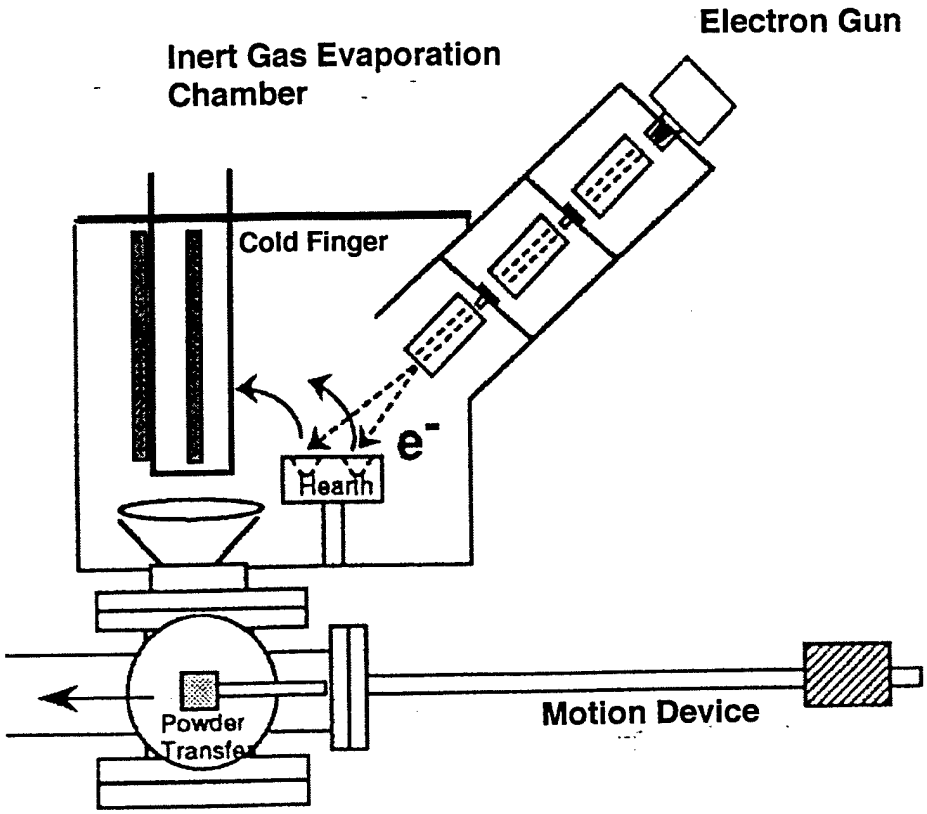

Figure 5 Figure shows the schematic view of inert gas evaporation chamber fitted with an Electron beam

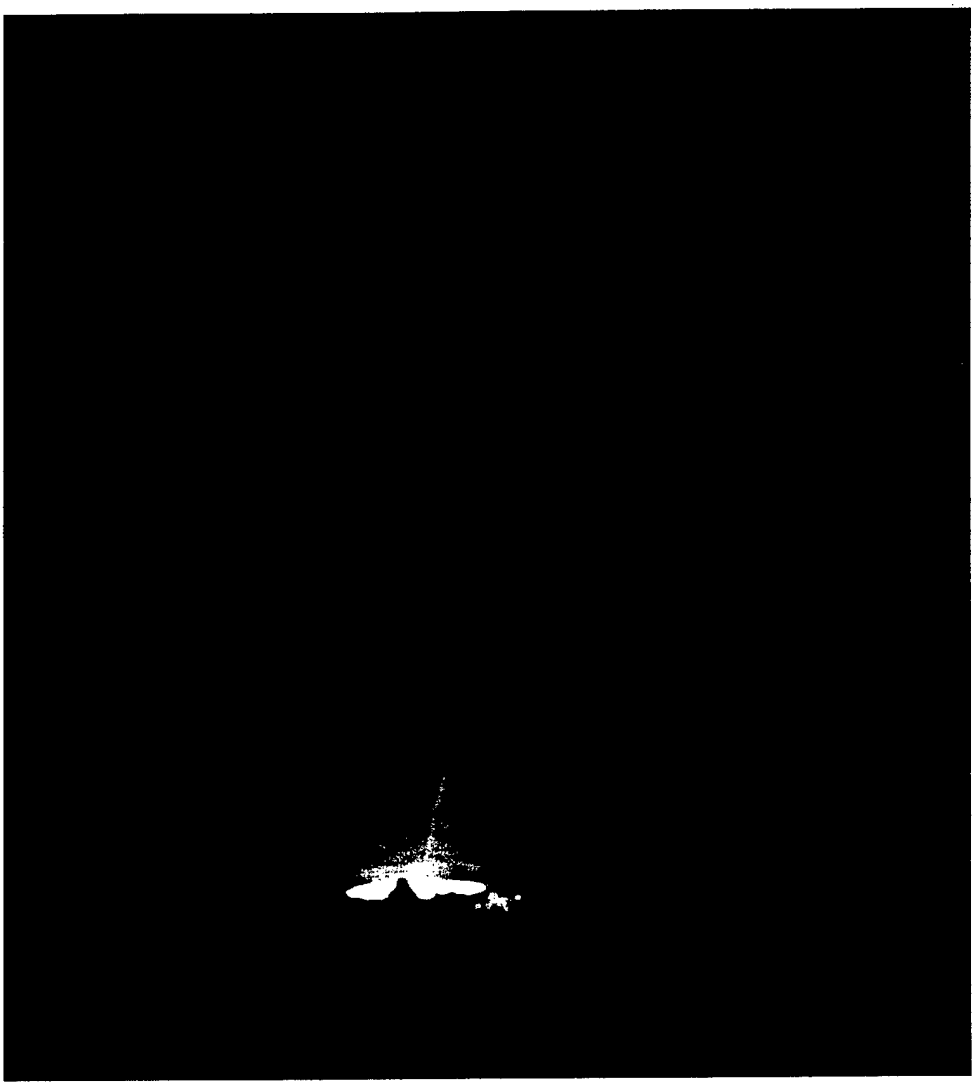

Figure 6 View of the hearth showing simultaneous evaporation of two source materials

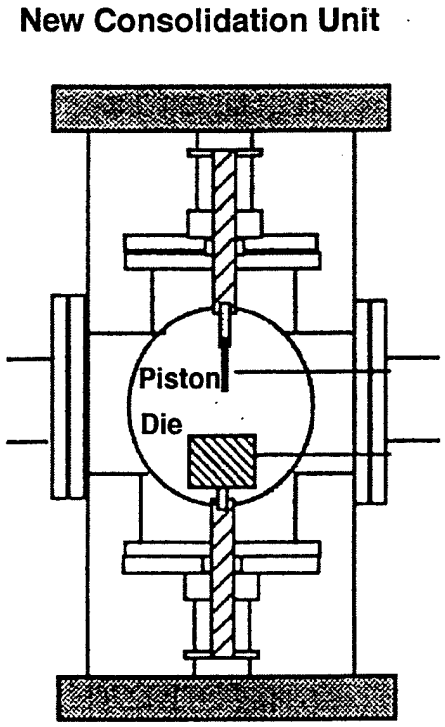

Figure 7 Schematic view of new consolidation unit connected directly to Inert gas evaporation chamber

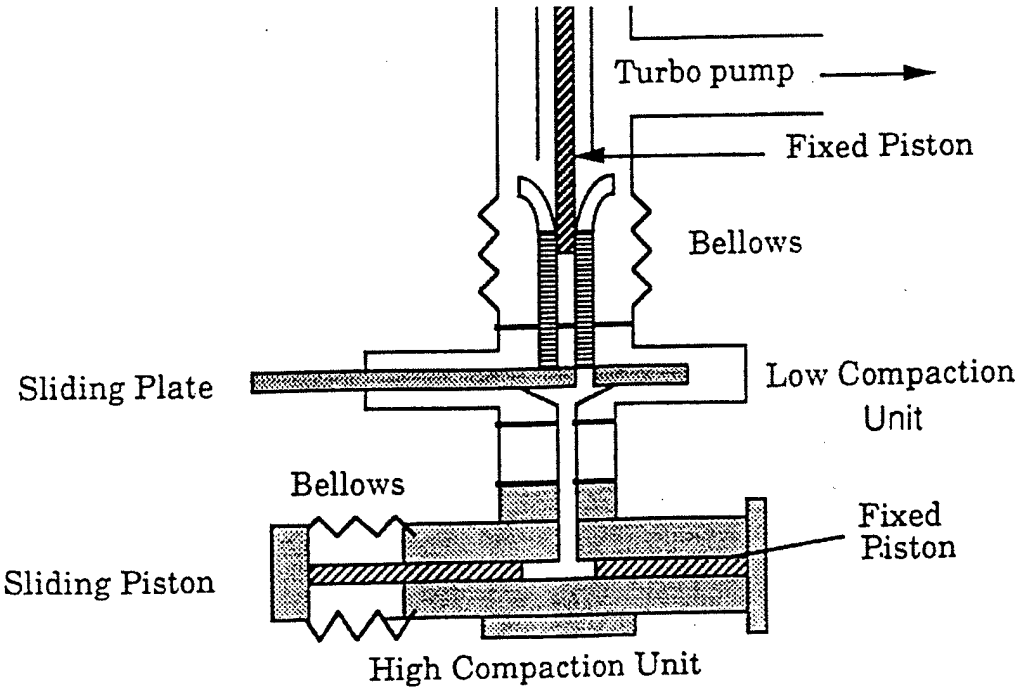

Figure 8 Schematic view of old consolidation unit showing how and high compaction units

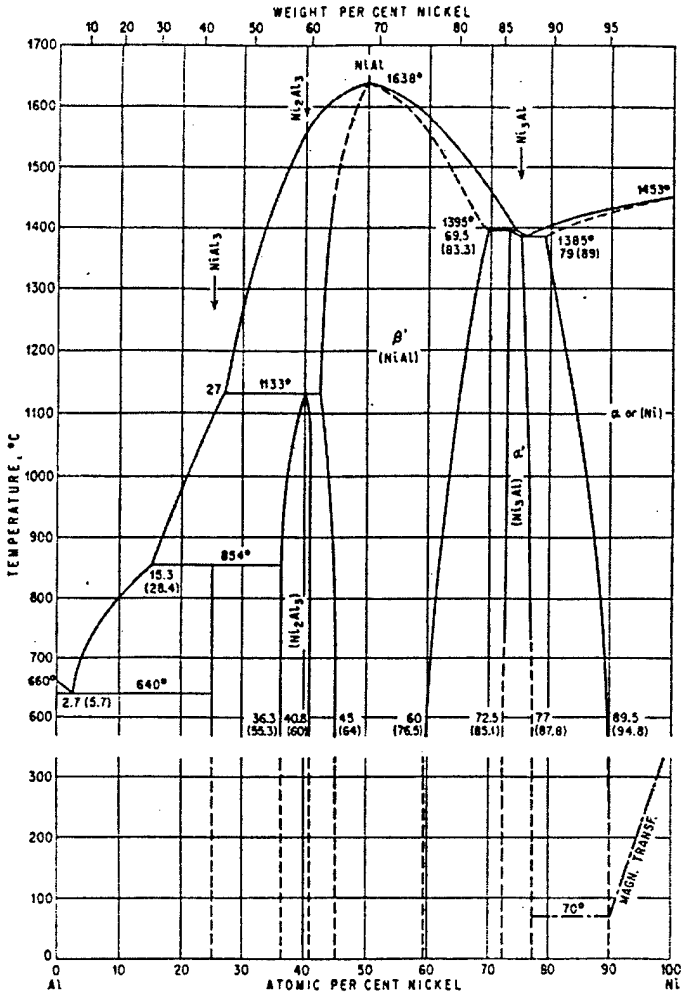

Fig. 68. Al-Ni. (See also Fig. 69.)

Figure 9 Phase diagram of NiAl

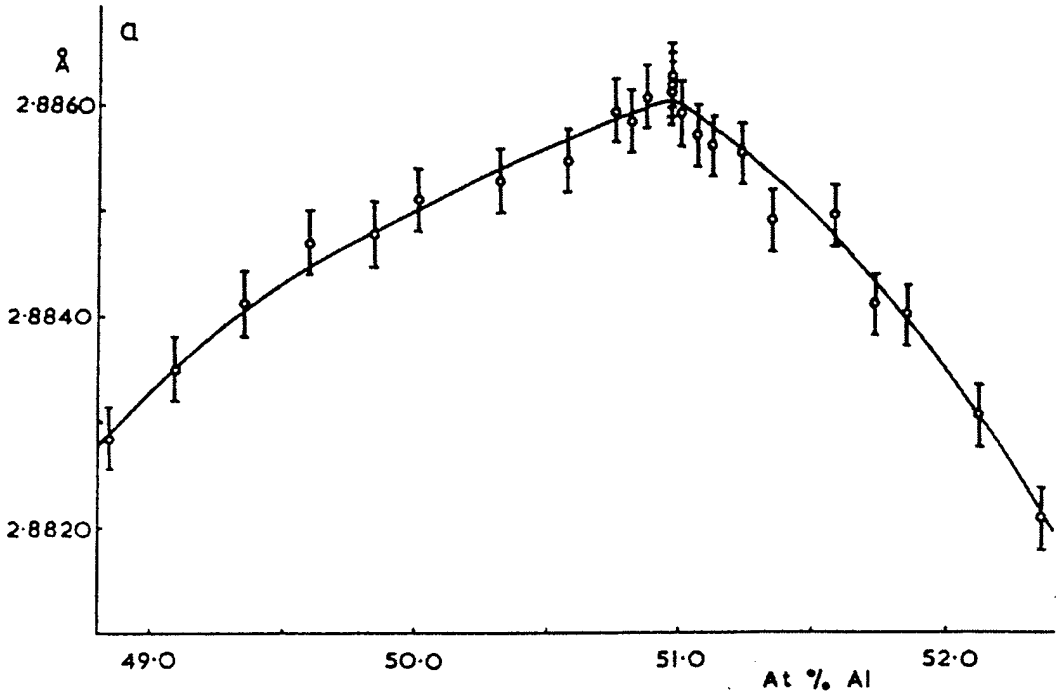

Figure 10 The observed variation of lattice parameter with initial composition for NiAl.

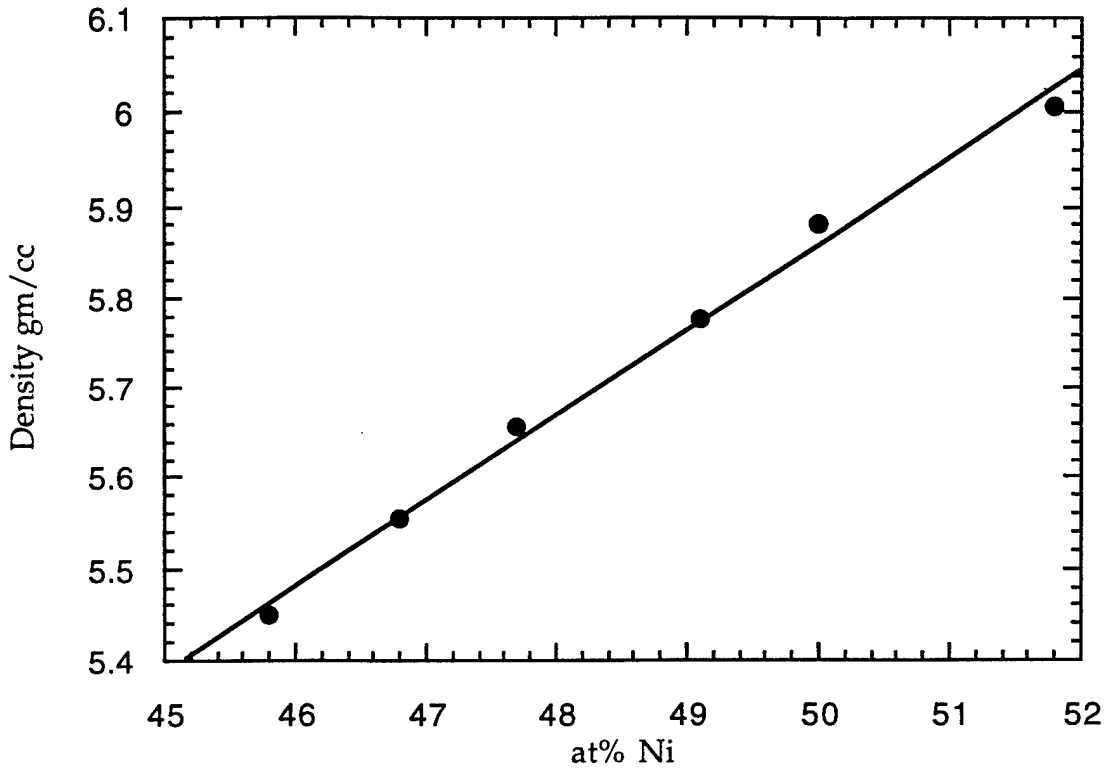

Figure 11 Variation of density as a function of Ni content

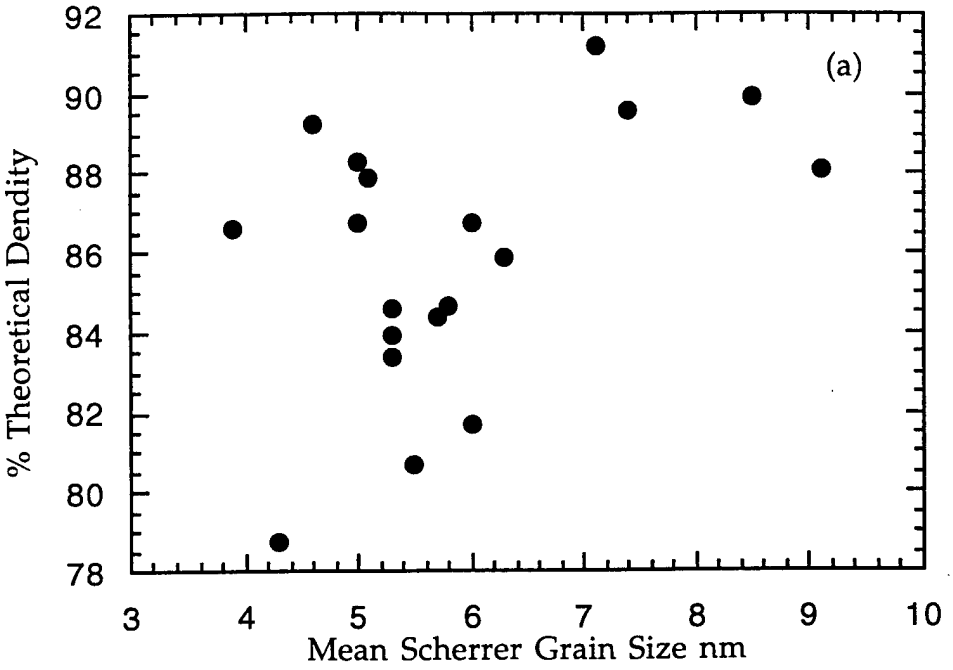

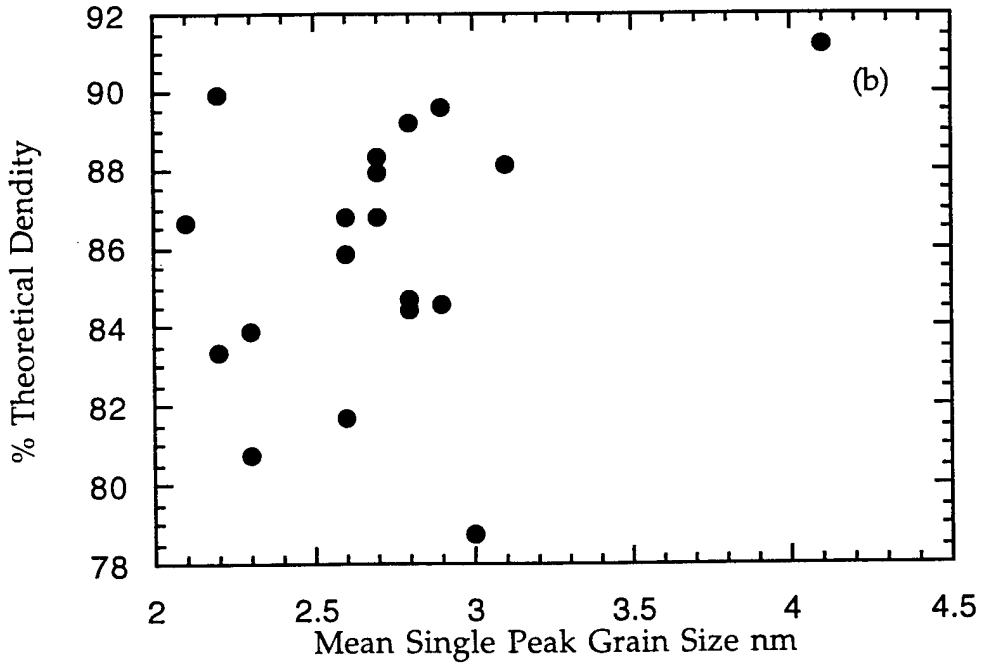

Figure 12 % theoretical density of specimens with composition in the single phase region is ploted against the (a) mean grain size obtained by Scherrer method and (b) mean single peak grain size

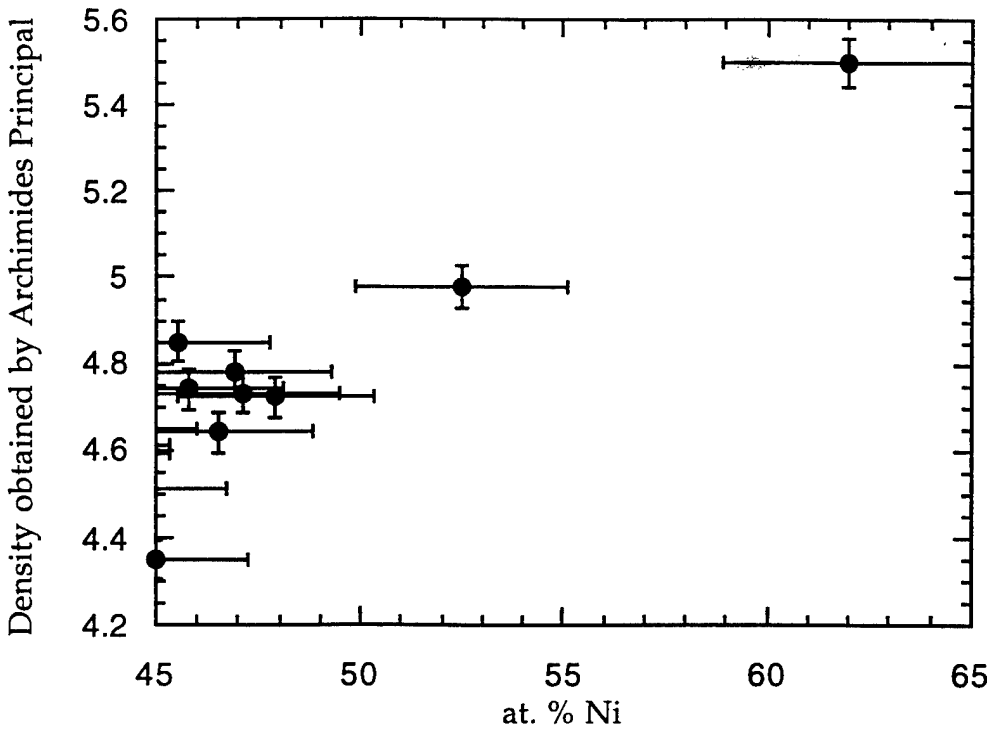

Figure 13 Density obtained by Archimidis Principal for specimens in the as compacted state against the at. % Nickel content obtained by SEM EDS analysis

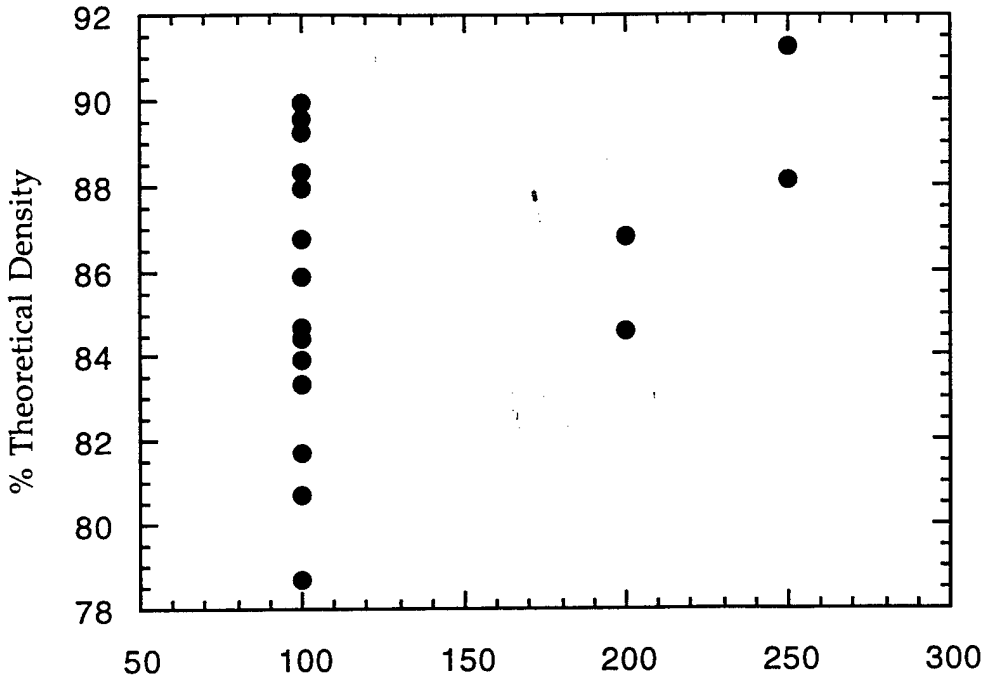

Figure 14 The densities of specimens in the as compacted state plotted against dietemperature used during compaction

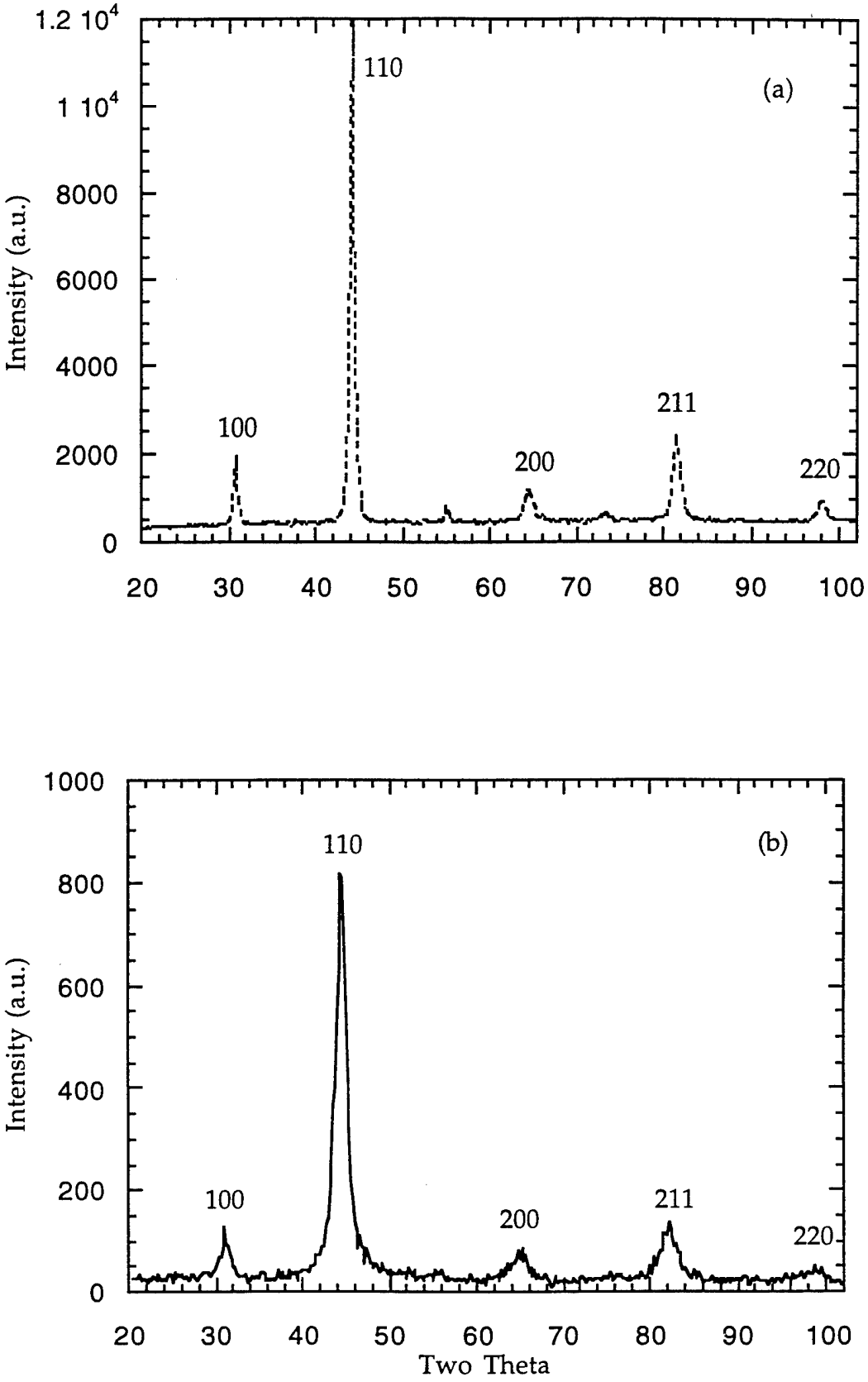

Figure 15 Representative XRD scans of (a) standard coarse grained NiAl and (b) nanocrystalline NiAl samples

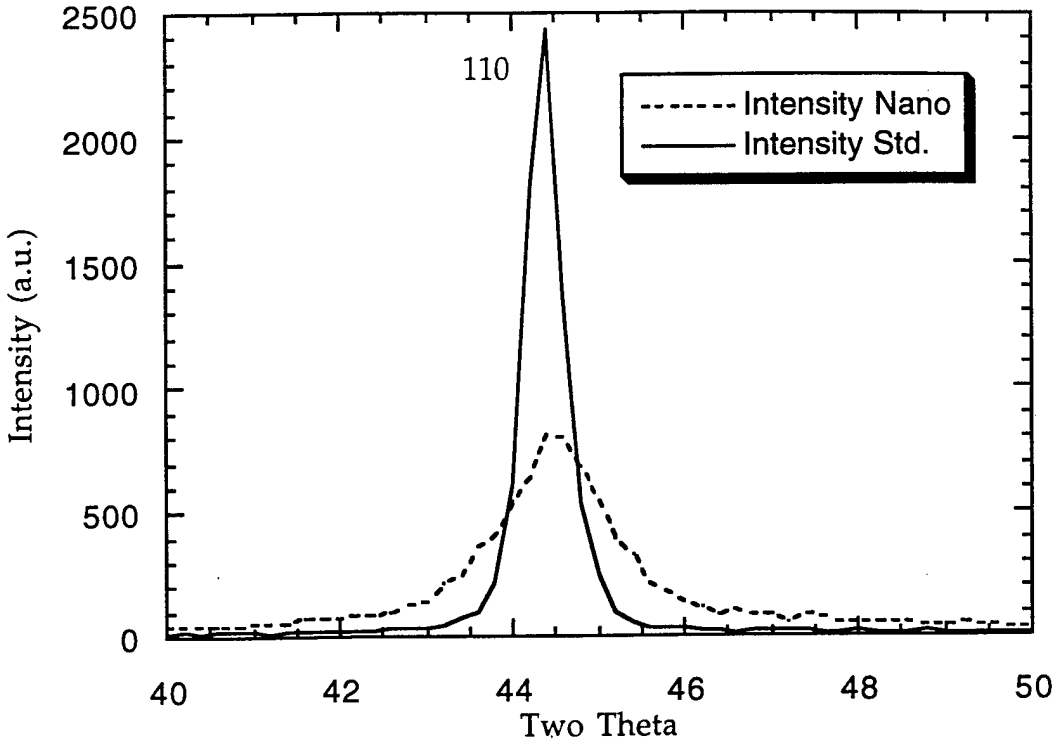

Figure 16 Example of grain size broadening of the (110) XRD profile for nanocrystalline NiAl shown with the corresponding NIAl coarse grain standard

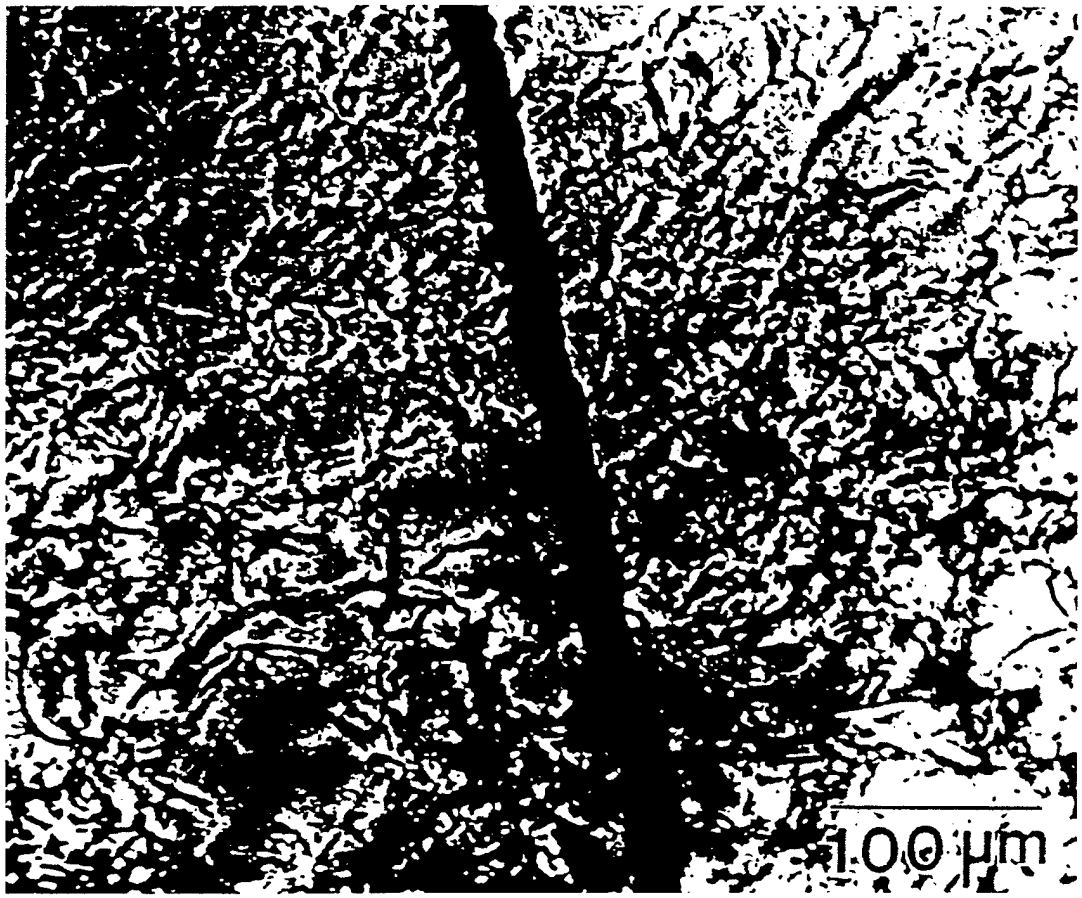

Figure 17 Optical photomicrograph showing the surface features of nanocrystalline NiAl. Note the presence of low compacted rim

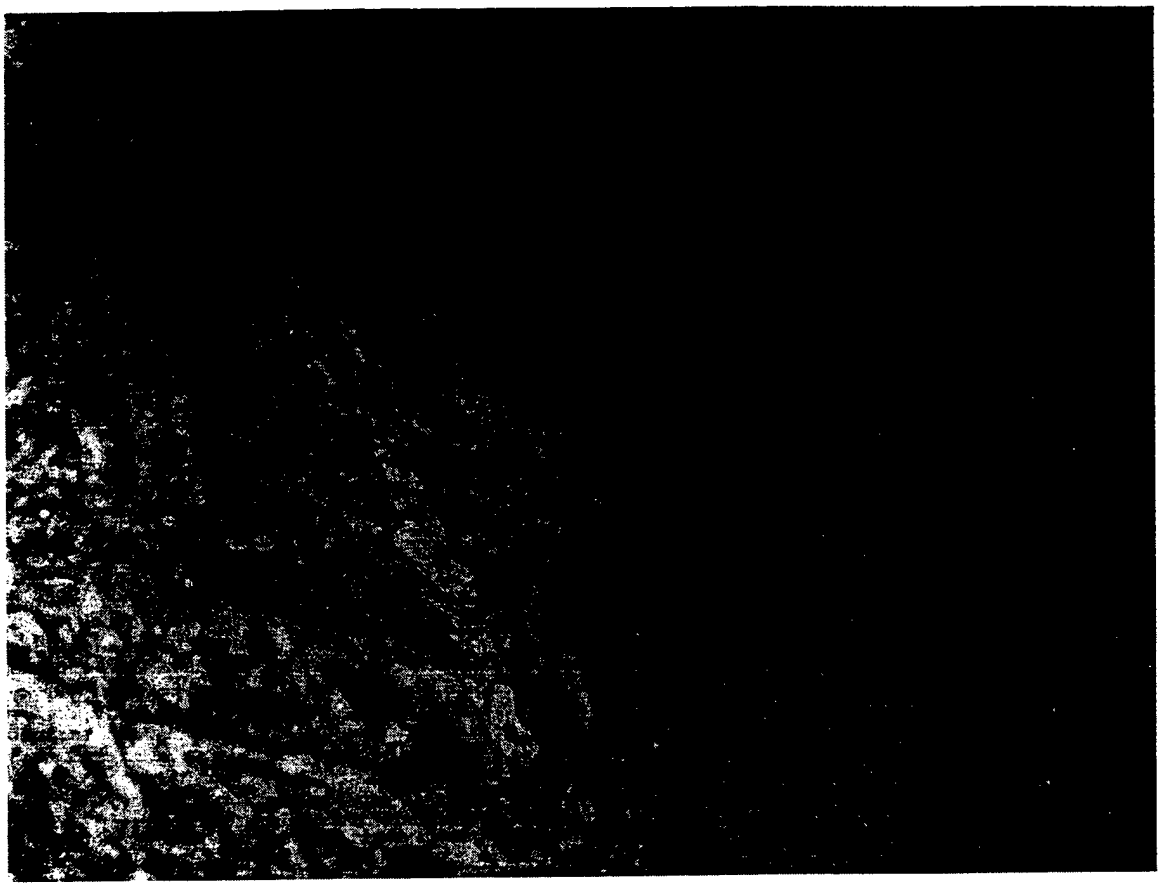

Figure 18 Optical photograph of as-consolidated nanocrystalline NiAl showing no cracks or regions of low compacted rim

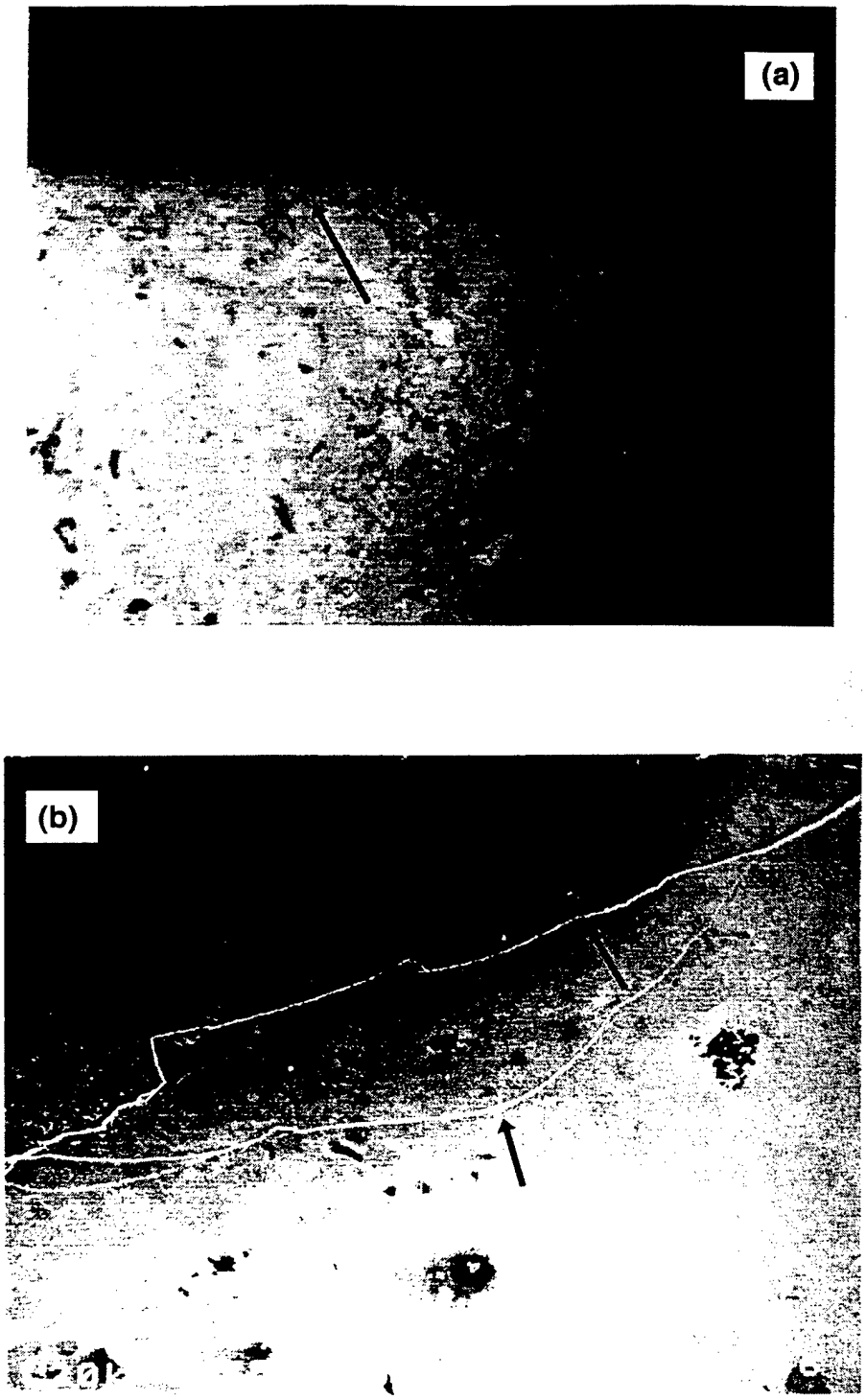

Figure 19 Arrows pointing out cracks developed in specimens.
(a) Optical micrograph (b) SEM photo micrograph

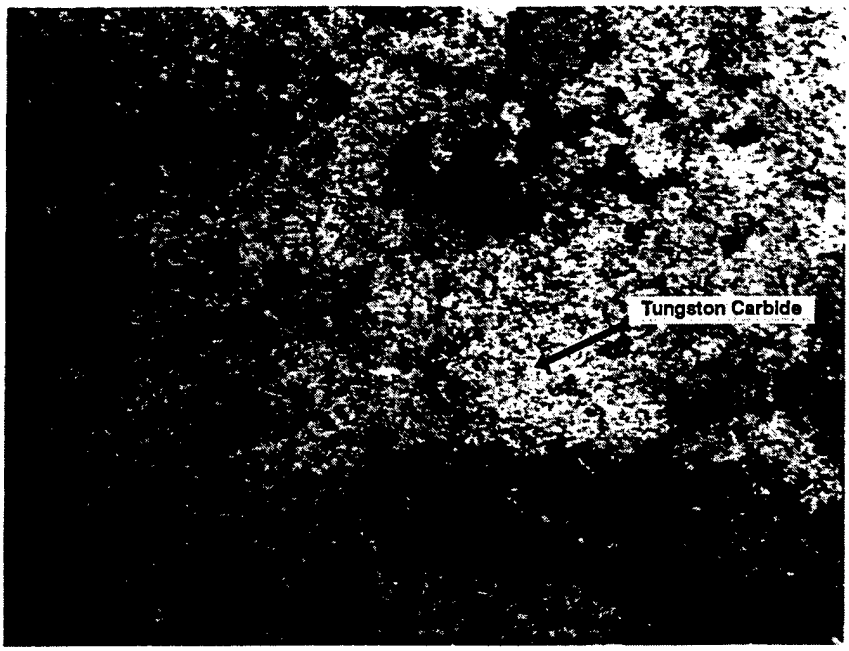

Figure 20 Optical micrograph of Nanocrystalline NIAl. The surface is contaminated with Tungston Carbide.

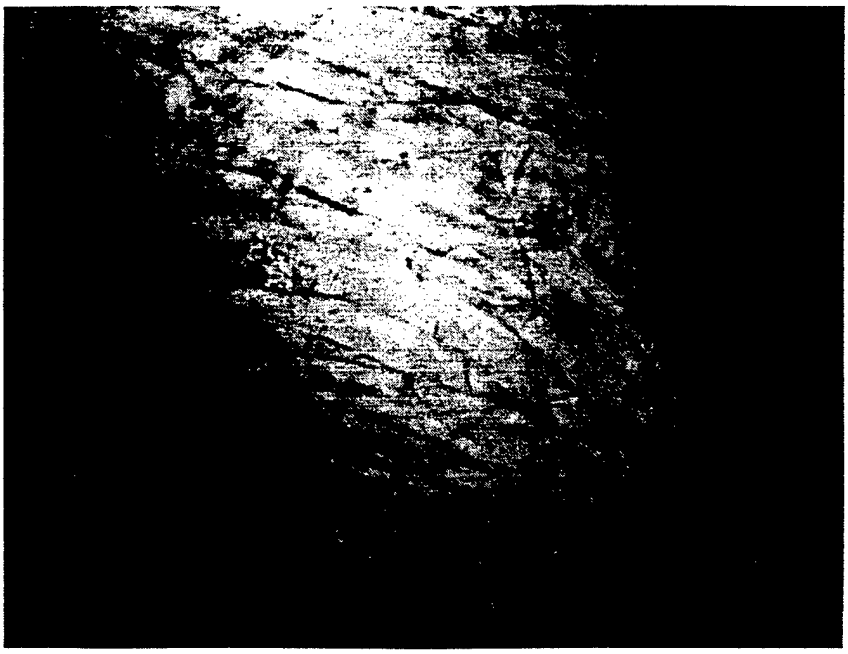

Figure 21 String like features present in most of the specimens with random orientation

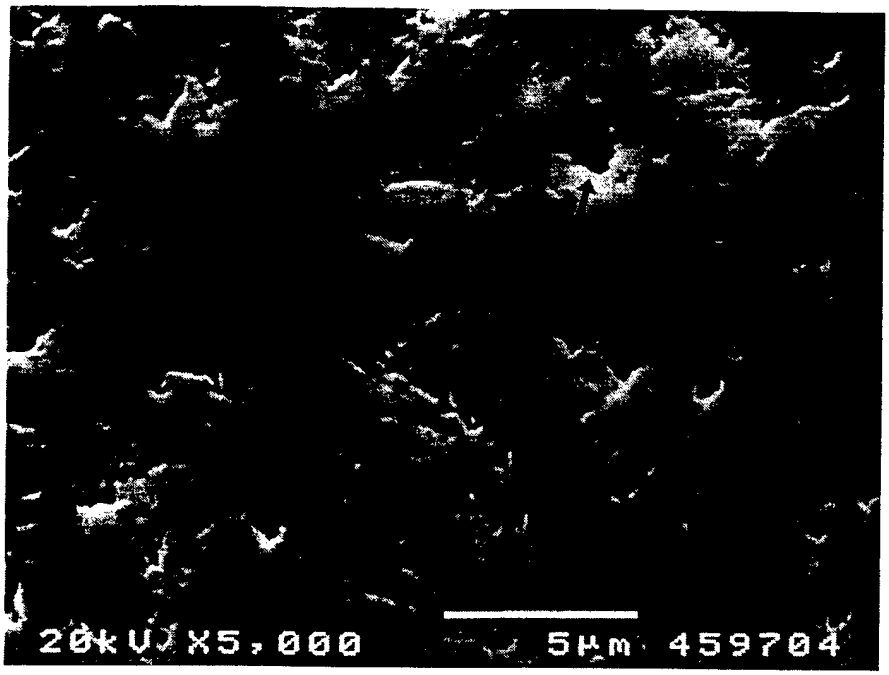

Figure 22 SEM photo micrograph shows prosity present in specimens in as-consolidated state

6. REFERENCES:

1 H. Gleiter, in Deformation of PolVcrystals: Mechanisms and Microstructures, edited by N. Hansen et al., (Ris~ National Laboratory, Roskilde, Denmark, 1981) p. 15.

2 R. Birringer, U. Herr, and H. Gleiter, "Nanocrystalline materials - a first report," Suppl. Trans. Jpn. Inst. Metall. 27, 43-52 (1986).

3 R. Birringer, H. Gleiter, H-P. Klein, and P. Marquardt, "Nanocrystalline materials - an approach to a novel solid structure

4 R. W. Siegel, Mat. Sci and Tech. 15, 583 (1991)

5 R. Birringer, Mat. Sci and Engr. A117, 33 (1989)

6 H. Gleiter, Prog. Mater. Sci. 33, 223 (1989).

7 H. Hahn and R. S. Averback, J. Am. Ceram. Soc. 74, 2918 (1991).

8 P. H. Shingu, B. Huang, U. J. Kuyama, K. N. Ishihard, and S. Nasu, in New Materials by Mechanical Alloying Techniques, E. Arzt and L. Schultz, eds., (Deitscje Gesellschaft fur Metallkunde, Oberursel, FRG, (1989) pp. 319-326.

9 G.W. Nieman, J. R. Weertman and R. W. Siegel, J. Mater. Res. 6, 1012 '(1991).

10 A.M. E1-Sherik, U. Erb, G. Palumbo and K. T. Aust, Scripta Metall. et Mater. 27, 1185 (1992).

11 G.D. Hughes, S. D. Smith, C. S. Pande, H. R. Johnson and R. W. Armstrong, Scripta Metall. 20, 93 (1986).

12 M. N. Rittner, J. A. Eastman, and J. R. Weertman, Scripta Metall et Mater. 31, 841 (1994)

13 G. W. Nieman, J. R. Weertman and R. W. Siegel, Scripta Metall., 2013 (1989).

14 W. Schlump and H. Grewe, in New Materials by Mechanical Alloying Techniques, E. Arzt and L. Schultz, eds., (Deitscje Gesellschaft fur Metallkunde, Oberursel, FRG, 1989) pp. 307-318.

15 K. Hayashi and H. Etoh, Mater. Trans., JIM 30, 925 (1989).

16 S. J. Suh Ph.D. Dissertation, Illinois Institute of Technology, Chicago, IL (1994)

17 H. J. Fecht, in Nanophase Materials: Synthesis-Properties-Applications, G. Hadjipanayis and R. W. Siegel, eds. (Kluwer, Dordrecht, 1994) p. 125.

18 C. G. Granqvist and R. A. Buhrman, J. Appl. Phys. 47, 2200 (1976).

19 J. R. Pierce, Theory and Design of Electron Beams, D. Van Nostrand Co., Inc., Princeton, NJ (1954)

20 J. A. Eastman, L. J. Thompson, and D. J. Marshall,

21 J. Hirskhorn, Introduction to Powder Metallurgy, (Amer. Powder Metallurgy Inst., N.Y., 1969), p. 119.

22 G. W. Niemen, Ph.D. Dissertation, Northwestern University, Evanston, IL (1991)

23 G. E. Fougers, Ph.D. Dissertation, Northwestern University, Evanston, IL (1995)

24 E. Y. Gutmanas, Prog. Mater. Sci. 34, 261 (1990).

25 D. B. Miracle, Acta. Metall. Mater. 41, 649 (1993)

26 A. Taylor and N. J. Doyle, J. Appl. Crystallogr. 5, 201 (1972)

27 M. J. Cooper, Phil. Mag. 89, 805 (1963)

28 N. Rusovic and H. Warlimont, Physica Status Solidi (a) 44, 609 (1977)

29 M. R. Harmouche and A. Wolfenden, J. Test. Eval. 15, 101 (1987)

30 T. Hughes, E. P. Lautenschlager, J. B. Cohen and J. O. Brittain, J. Phys. Chem. 42, 3705 (1971)

31 A. J. Bradley and A. Taylor, Proc. R. Soc. A 159, 56 (1937)

32 L. N. Guseva, Dokl. Acad. Nauk. USSR 77, 415 (1951)

33 H. Jacobi and H. J. Engell, Acta Metall. 19, 701 (1971)

34 G. W. West, Physica Status Solidi (a) 20, 647 (1973)

35 P. Georgopoulos and J. B. Cohen, Scripta Metall. 11, 147 (1977)

36 A. H. Chokshi, A. Rosen, J. Karch and H. Ghiter, Scripta. Metall. 23, 1679 (1989)

37 Hahn, J. A. Eastman, and R. W. Siegel, "Processing of Nanophase Ceramics," Ceramic Trans. 1B, 1115-1122 (1988).

38 R.W. Siegel and H. Hahn, "Nanophase materials," in Current Trends in the Physics of Materials, ed. by M. Yussouff, (World 39

39 G. W. Nieman, J. R. Weertman, and R.W. Siegel, "Tensile strength and creep properties of nanocrystalline palladium," Scripta Metall. et. Mater. 24, 145-150 (1990).

40 G.W. Nieman, J. R. Weertman, and R.W. Siegel, "Microhardness of nanocrystalline palladium and copper produced by inert-gas

condensation," Scripta Metall. 23, 2013-2018 (1989).

41 K. Kimato, Y Kamiya, M. Nonoyama, and R. Uyeda, "An electron microscope study of fine metal particles prepared by evaporation in argon gas at low pressure," Jpn. J. Appl. Phys. 2, 702-713 (1963)

42 K. Kimato, and I. Nishida, "An electron microscope and electron diffraction study of fine smoke particles prepared by evaporation in argon at lo~v pressures (II)," Jpn. J. Appl. Phys. 6, 1047-1059 (1963).

43 C. G. Granqvist and R. A. Buhrman, "Ultrafine metal particles," J. Appl. Phys. 47, 2200-2219 (1976); R. A. Buhrman and C. G. Granqvist, "Log-normal size distributions from magnetization measurements on small superconducting A1 particles," J. Appl. Phys. 47, 2220-2222 (1976).

44 y. Mizushima, "Entstehungmechanismus schwarzer Metallauf dampfschichten," Z. Naturforsch. A16, 1260-1261 (1961).

45 L. Fritsche, F. Wolf, and A. Schaber, "Zur Struktur und Entstehung schwarzer Wismutaufdampfschichten," Z. Naturforsch. A16, 31-36 (1961).

46 A. R. Tholen, "On the formation and interaction particles,"'Acta Metall. 27, 1765-1778 (1979)

47 E. Hellstern, H. J. Fecht, Z. Fu and W. L. Johnson, "Structural and thermodyn~mic properties of heavily mechanically deformed Ru and RuA]," J. Appl. Phys. 65,305-310 (1989).

48 M.R. Fitzsimmons, J. A. Eastman, M. M~iller-Stach, and G. Wallnet, "Characterization of nanocrystalline Pd by x-ray diffraction techniques," submitted for publication (1991); "Characterization of nanocrysta]line Pd by x-ray diffraction and EXAFS," Proc. of the Acta Metallurgica Symposium on "Materials With Ultrafine Microstructures," Atlantic City, NJ (1991), in press.

49 D.J. Deputy, unpublished M.S. thesis, Northwestern University (1989); D. J. Deputy, D. N. Seiclman, W. P. Halperin, W. J. Krauss, and H.Gleiter, "Characterization of nanograined metals," in Clusters And Cluster-Assembled Materials, edited by Robert S. Averback, J. Benholic, and David L. Nelson, Mater. Res. Soc. Syrup. Proc. 206 (1991)

50 B.E. Warren, X-ray Diffraction, (Addison-Wesley, Reading, MA,1969) p. 251

51 L.H. Schwartz and J. B. Cohen, Diffraction from Materials, 2nd ed., (Springer-Verlag, Berlin, 1987) p..372.

52 A. Guinier, X-ray Diffraction In Crvsta]s, Imperfect Crystals and Amorphous Bodies, (W. H. Freeman and Co., San Francisco, (1970) p. 121.

53 A.J.C. Wilson, Elements of X-ray Crvstallography, (Addison-Wesley, Reading, MA, 1970) pp. 210-215.

54 B.D. Cullity, Elements of X-ray Diffraction, 2nd ed., (Addison-Wesley, New York,1978) pp. 99-103.

55 A. R. Tholen, in Nanophase Materials: Synthesis-Properties-Applications, G. Hadjipanayis and R.W. Siegel, eds. (Kluwer, Dordrecht, 1994) p. 63.

56 G. W. Nieman and J. R. Weertman, in Proceedings of the Morris E. Fine Symposium, P. K. Liaw et at., eds., (TMS, Warrendale, PA, (1990) p. 243.

57 P. G. Sanders, personal communication, 1995.

58 S. Enzo, G. Fagherazzi, A. Benedetti and S. Polizzi, "A profile-fitting procedure for analysis of broadened x-ray diffraction peaks. I. Methodology," J. Appl. Cryst. 21,536-542 (1988); A. Benedetti, G. Fagherazzi, S. Enzo, and M. Battagliarin, "A profile-fitting procedure for analysis of broadened x-ray diffraction peaks. II. Application and discussion of the methodology," J. Appl. Cryst. 21,543-549 (1988).

59 G.J. Stanisz, J. M. Holender, and J. Soltys, "X-ray diffraction profile analysis of powdered samples," Powder Diff. 4, 70-73 (1989).

60 R. L. Rothman and J. B. Cohen, in Advances in X-Ray Analysis, J. B. Cohen et al., eds., 12, 208 (1969)

61 K. Kimoto, J. Phys. Soc. Japan (5), 47, 2200 (1976)